Section 2 Plasma Physics

Chapter 1. Plasma Dynamics

Academic and Research Staff

Professor George Bekefi, Professor Abraham Bers, Professor Bruno Coppi, Professor Miklos Porkolab, Professor Jonathan S. Wurtele, Dr. Chiping Chen, Dr. Shien-Chi Chen, Dr. Paolo Detragiache, Dr. Stefano Migliuolo, Dr. Abhay K. Ram, Dr. Barrett Rogers, Dr. Linda E. Sugiyama, Edward W. Fitzgerald, Ivan Mastovsky

Visiting Scientists and Research Affiliates

Dr. Gregory A. Benford, Dr. Carson C. Chow,[1] Dr. Vladimir Fuchs,[2] Dr. Eli Jerby, Dr. Pallavi Jha, Dr. Cesar Meirelles-Filho,[3] Dr. Marco Nassi,[4] Dr. Leonid E. Zakharov[5]

Graduate Students

Neer R. Asherie, Palmyra E. Catravas, Manoel E. Conde, David S. Gloss, Wen Hu, Alexander Matusis, Michael C. Moldoveanu, Gregory E. Penn, Caterina Riconda, Todd H. Rider, Steven D. Schultz, Jared P. Squire, Richard E. Stoner, Luigi Vacca, Jesus Noel Villaseñor, Pavel S. Volfbeyn

Undergraduate Students

Jonathan C. Doan, Todd A. Hay, Hana Ohkawa, Vladislav Portnoy, Kenneth N. Ricci

Technical and Support Staff

Felicia G. Brady, Laura B. Doughty, Kerry L. Gafney, Catherine Lorusso

1.1 Relativistic Electron Beams

Sponsors

National Science Foundation
Grant ECS-89-02990
U.S. Air Force - Office of Scientific Research
Grant AFOSR 89-0082-C
U.S. Army - Harry Diamond Laboratories
Contract DAAL02-89-K-0084
Contract DAAL02-92-K-0037
U.S. Department of Energy
Contract DE-AC02-90ER-40591
U.S. Navy - Office of Naval Research
Grant N00014-90-J-4130

Project Staff

Professor George Bekefi, Professor Jonathan S. Wurtele, Ivan Mastovsky, Dr. Chiping Chen, Dr. Shien-Chi Chen, Dr. Eli Jerby, Dr. Pallavi Jha, Dr. Gregory A. Benford, Palmyra E. Catravas, Manoel E. Conde, Wen Hu, Alexander Matusis, Richard E. Stoner, Pavel S. Volfbeyn, Jonathan C. Doan, Todd A. Hay, Kenneth N. Ricci

1.1.1 Frequency Shifting Phenomena In Free Electron Lasers - Experiment

Frequency upshifting of an electromagnetic wave incident on a rapidly time varying plasma medium is of considerable interest recently. Such upshifting can occur as a result of a time-dependent dielectric

---

1 University of Colorado, Boulder, Colorado.

2 Centre Canadien de Fusion Magnétique (CCFM), Quebec, Canada.

3 Universidade de São Paulo, Brazil.

4 Politecnico di Milano, Milan, Italy.

5 Kurchatov Institute of Atomic Energy, Moscow, Russia.

coefficient caused by changes in plasma density,[6] or as a result of a rapidly moving plasma-vacuum boundary.[7] Prior studies have been confined to cases in which the dielectric is essentially a passive medium; that is, the amplitude of the wave propagating through it is constant in time and space. In this paper we report what we believe are the first frequency shift measurements in an active, lasing medium in which the wave amplitude exhibits exponential growth. Here, the time-varying dielectric medium is modeled as an interaction between the pulsed relativistic electron beam of the free electron laser (FEL), the magnetic wiggler, and the copropagating electromagnetic wave launched into the system. The detailed theoretical and computational modeling by Shvets and Wurtele is described elsewhere.[8]

A schematic of the FEL[9] amplifier is shown in figure 1a. A mildly relativistic electron beam (750 keV) is generated by a Marx capacitor bank (Physics International Pulserad 110 Å). The electrons are emitted from a hemispherical graphite cathode by an explosive field-emission process. The graphite anode acts as an emittance selector, allowing only a small fraction of the current (90 Å) to propagate through its 2.54-mm radius and 62-mm-long aperture.

The 50-period bifilar helical wiggler produced by current-carrying helical wires has a period of 3.18 cm and provides a magnetic field of uniform amplitude whose magnitude on axis is adjustable up to 1.8 kG. The wiggler field intensity is slowly increased over the initial six periods, providing an adiabatic input for the electron beam. The system, including the gun, is immersed in a uniform axial guide magnetic field generated by a solenoid. The intensity of this field can be varied up to a maximum of 11.6 kG.

The 2-m-long stainless-steel drift tube has an internal radius of 0.51 cm and acts as a cylindrical waveguide whose fundamental TE_{11} mode has a cutoff frequency of 17.2 GHz. The system is designed to operate in this lowest waveguide mode.

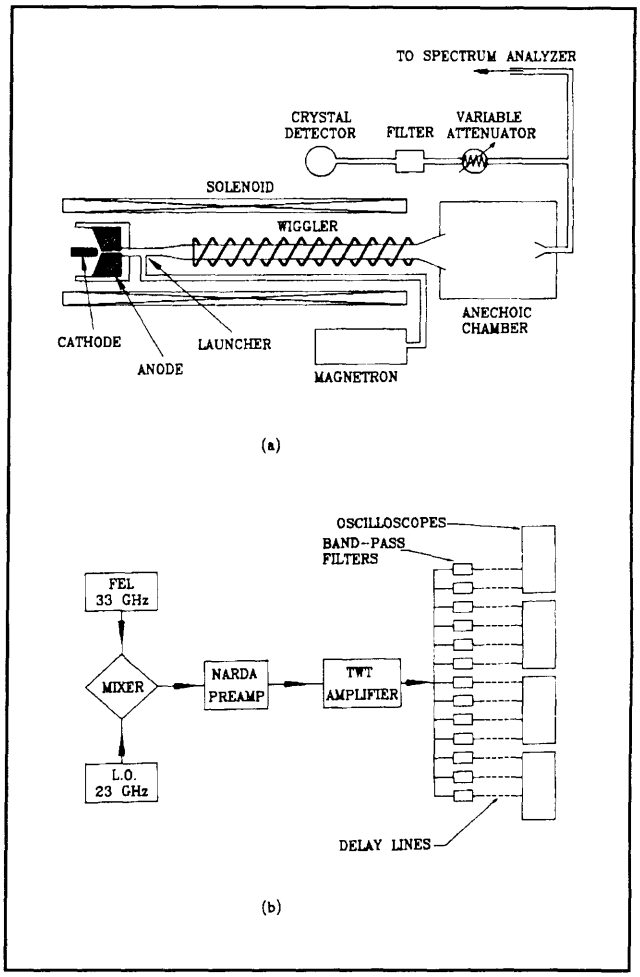

Figure 1. (a) Free electron laser set-up (b) schematic of the spectrum analyzer.

A high-power magnetron operating at 33.39 GHz is the input power source for the FEL amplifier. The wave launcher consists of a short section of circular waveguide of radius 0.31 cm into which ~12 kW of power is coupled from a standard Ka-band rectangular waveguide. This section of circular waveguide supports only the fundamental TE_{11} mode for the operating frequency. Its radius is then adiabatically increased to the radius of the drift tube. A linearly polarized wave is thereby injected into the interaction region. Half of the incident

---

6 S.C. Wilks, J.M. Dawson, and W.B. Mori, *Phys. Rev. Lett.* 61: 337 (1989); C.J. Joshi, C.E. Clayton, K. Marsh, D.B. Hopkins, A. Sessler, and D. Whittum, *IEEE Trans. Plasma Sci.* 18: 814 (1990); V.R. Goteti and D.K. Kalluri, *IEEE Trans. Plasma Sci.* 17: 828 (1989); D.K. Kalluri, *IEEE Trans. Antennas Propag.* 37: 1638 (1989).

7 W.B. Mori, *Phys. Rev. A* 44: 5118 (1991); P. Sprangle, E. Esarey, and A. Ting, *Phys. Rev. A* 41: 4463 (1990); H.C. Kapteyn and M.M. Murnane, *J. Opt. Soc. Am. B* 8: 1657 (1991); R.L. Savage Jr., W.B. Mori, C. Joshi, T.W. Johnston, and G. Shvets, Dept. of Electr. Eng., UCLA, Report No. PPG-1422 (1992).

8 G. Shvets and J. Wurtele, submitted to *Phys. Fluids.*

9 M.E. Conde and G. Bekefi, *Phys. Rev. Lett.* 67: 3082 (1991); M.E. Conde and G. Bekefi, *IEEE Trans. Plasma Sci.* 20: 240 (1992).

power, with the correct rotation of the electric-field vector of the amplified circularly polarized wave, participates in the FEL interaction.

The output power from the FEL is transmitted by means of a conical horn into a reflection free "anechoic chamber." A small fraction of the radiation is then collected by a receiving horn, passes through precision calibrated attenuators, and a 1.7-GHz-wide band-pass filter. The power level is finally determined from the response of a calibrated crystal detector.

The spatial growth of the electromagnetic wave intensity is determined from the measurement of the output power as a function of the length of the interaction region. This length is varied by changing the distance that the electron beam is allowed to propagate in the drift tube. Application of a strong transverse magnetic field locally is sufficient to deflect the electrons into the waveguide wall and thereby terminate the interaction at that point. The results of such measurements are illustrated in figure 2 which shows an initial exponential growth of the signal intensity, followed by nonlinear saturation at a power level of ~6 MW.

The frequency spectrum of the output power is determined by a heterodyne technique. A crystal rectifier is used as a mixer for the 33 GHz FEL radiation and for radiation from a variable frequency 23 GHz local oscillator. The resulting beat wave is amplified and sent to an array of band-pass waveguide filters. Thus, the calibrated response of the various channels provides, on a single shot basis, a direct histogram of output power in terms of radiation frequency.

A schematic of the experimental setup used to measure the frequency spectrum is shown in figure 1b. An Alfred 650 sweep oscillator is used as a local oscillator, generating ~6 mW at 23.39 GHz. This signal is combined in a magic tee with the FEL signal (previously attenuated to the appropriate milliwatt level) and then sent to a crystal rectifier (HP R422A). The nonlinear response of this crystal gives rise to the beat wave of the two signals, with a frequency of 10 GHz. This beat wave is then amplified by a Narda 60164 solid state amplifier and by a Logimetrics TWT, and finally sent to the filter bank. The bank consists of 32 waveguide band-pass filters adjacent in frequency and each one 80 MHz wide. These channels are fed in parallel and each one has its own rectifier crystal (HP 33330B). Thus, the calibrated response of this array of rectifiers gives, on a single shot basis, the frequency spectrum of the output power.

There are two factors limiting the number of channels that can actually be used. The first one is the

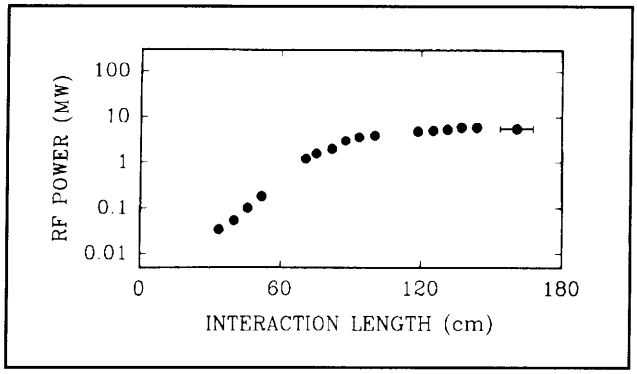

Figure 2. FEL output power as a function of the interaction length. Beam energy 750 keV; beam current 90 Å; axial guide magnetic field 4.06 kG; wiggler magnetic field 0.63 kG.

bandwidth of the TWT amplifier, from 9.5 to 10.5 GHz, allowing only 13 channels to be used. The other limitation is the number of available oscilloscopes to monitor the filter bank channels. This second problem is solved by using delay lines to give temporal separation between channels, such that four of them can be added in a single oscilloscope. The measured attenuation of each of these delay lines has to be taken into account in the analysis of the data.

The frequency spectrum in the saturation region, corresponding to a measurement with a full length wiggler of ~180 cm (see figure 2) is shown in figure 3a. We observe that the spectrum is shifted from the input magnetron frequency. Its full width at half maximum (FWHM) is less than 160 MHz. The 80 MHz width of each band-pass filter does not allow a resolution better than this, and, as a matter of fact, the short duration of the radiation pulse (~20 ns) limits the resolution to no better than ~50 MHz (dictated by $\Delta f\, \Delta t \approx 1$).

To see if the frequency shift occurs at all power levels, that is, in the exponential growth regime and in the saturated regime, we scan the output power as a function of interaction length and observe any frequency shifts. Figure 3b shows a scan of power versus interaction length (using the kicker magnet) from two adjacent channels of the filter bank, namely, the channel corresponding to the driver frequency and its higher frequency neighbor. The driver channel initially has the higher power, but it is surpassed by the other channel for longer interaction distances. From these measurements and measurements of the total power integrated over the 1.7 GHz frequency band (figure 2), we conclude that for short interaction lengths, that is, in the exponential growth regime, the RF power is predominantly at the channel centered around the input magnetron frequency of 33.39 GHz. However, when one reaches the nonlinear satu-

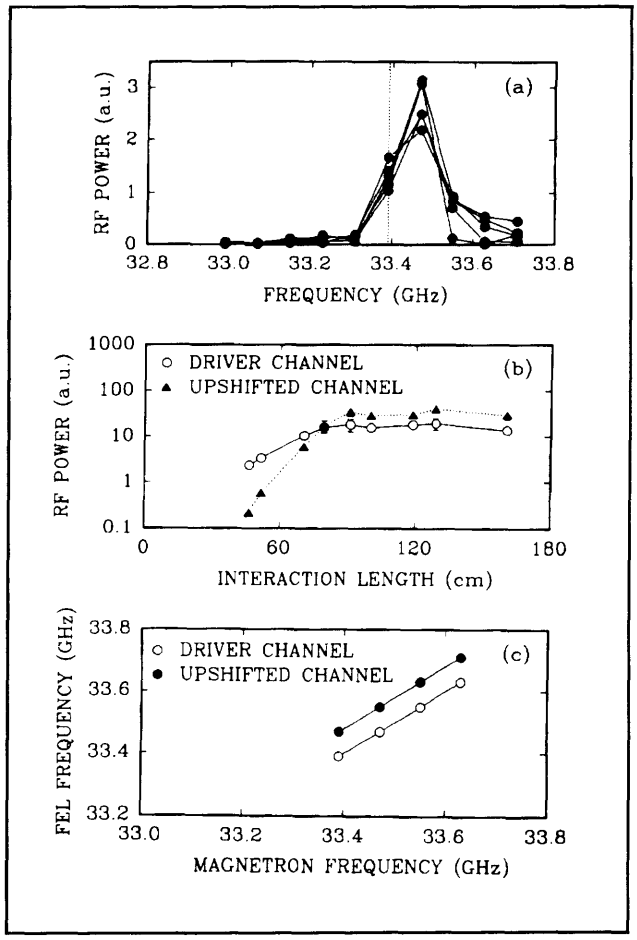

Figure 3. (a) Frequency spectrum of the FEL output power for five successive shots, for an interaction length of 180 cm; the dotted vertical line shows the input magnetron frequency. (b) RF power as a function of interaction length for two adjacent channels of the filter bank. (c) FEL frequency as a function of magnetron input frequency for an interaction length of 180 cm.

ration regime, the power is predominantly in the frequency upshifted channel centered around 33.47 GHz.

When the input magnetron frequency is varied, the frequency spectrum moves in proportion to the input frequency, but it is always shifted towards higher frequencies, as is shown in figure 3c.

In summary, we have observed frequency shifts in a pulsed free electron laser amplifier. One possible cause could be the presence of nonlinear excitation of side-band[10] instabilities which are often observed in the saturated regime of FELs. Since we observe frequency upshifting in both the exponential growth and saturation regimes (figure 3b) we rule this out as a cause of our observations. Another cause could be the presence of self-amplification of spontaneous emission (SASE) which occurs even in the absence of the magnetron driver. We rule out this effect for two reasons. First, our measurements[11] of SASE have shown that the intensity of the emission is about an order of magnitude lower than the intensity of the amplified signal (figure 2). Secondly, when we vary the magnetron frequency, the FEL emission frequency tracks the input magnetron frequency as illustrated in figure 3c.

Our observations are in qualitative agreement with computations modeled on the premise that the frequency shifting is the result of the rapid temporal variations, typically ~10 ns, of the voltage and current pulses of our FEL. This leads to temporal variations of the effective dielectric coefficient associated with the FEL interaction. The contributions to Δf are shown[12] to consist of two components. One can be attributed to "dielectric beam loading", that is, the temporal behavior of the right circularly polarized wave propagating through the relativistic electron beam. This is present even in the absence of the magnetic wiggler and leads to frequency downshifting. The other component is associated with the temporal variations of the slow ponderomotive wave excited by the presence of the magnetic wiggler, and yields a frequency upshift. The net of the two effects is a frequency upshift of ~100 MHz.

We note that the magnitude of the frequency upshifting or downshifting depends sensitively[12] on the relative temporal voltage and current histories of the relativistic electron beam. These may differ for different regimes of FEL operation. The aforementioned experiments were carried out in an FEL operating in the Group I regime. Frequency shifting was not seen in the Group II or in the Reversed Field regimes[13] which occur at much higher guide magnetic fields. To fully understand the differences in the observed frequency characteristics requires

---

[10] W.B. Colson, *Nucl. Instrum. Methods A* 250: 168 (1986); F.G. Yee, J. Masud, T.C. Marshall, and S.P. Schlesinger, *Nucl. Instrum. Methods A* 259: 104 (1987).

[11] M.E. Conde and G. Bekefi, *IEEE Trans. Plasma Sci.* 20: 240 (1992).

[12] G. Shvets and J. Wurtele, submitted to *Phys. Fluids.*

[13] M.E. Conde and G. Bekefi, *Phys. Rev. Lett.* 67: 3082 (1991); M.E. Conde and G. Bekefi, *IEEE Trans. Plasma Sci.* 20: 240 (1992).

monitoring the temporal beam voltage and current characteristics to a precision of the order of 1-2 ns, a task that has not been carried out to date.

Our frequency shift measurements were carried out in a Raman FEL *amplifier.* However, frequency shifts may also be important[12] in FEL oscillators. They could also be of practical interest in frequency chirping using carefully shaped voltage and current pulses of the relativistic electron beam.

1.1.2 Frequency Shifting Phenomena In Free Electron Lasers - Theory

The frequency shifting of light by a moving dielectric front and bulk ionization of gases has been extensively investigated both theoretically and experimentally. These studies have been restricted to passive dielectric systems—those which induce phase shifts but have negligible gain. An electromagnetic wave in an underdense plasma, with dielectric $\varepsilon = 1 - \frac{\omega_p^2}{\omega^2}$,

being the typical example. Similar physics can be expected in an active medium which exhibits both gain and phase shifts, such as the FEL. Since any frequency shift creates a phase shift, these shifts must be fully understood if the FEL is used as a driver for high gradient accelerators. They will place limits on the tolerable shot-to-shot jitter in system parameters. The frequency shifting mechanism also provides the first explanation of the way in which an FEL oscillator can adjust its frequency to changes in beam energy.

Two distinct parameter regimes, a high-power high-gain microwave amplifier and a low-gain infrared oscillator, have been studied in detail. A brief description of the amplifier analysis is given below; a detailed study is provided elsewhere. The theory is consistent with recent experiments[14] which report frequency upshifting in a FEL microwave amplifier.

The wave equation for the vector potential of the transverse EM wave including the FEL and plasma coupling is

$$\left(\frac{1}{c^2}\frac{\partial^2}{\partial t^2} - \frac{\partial^2}{\partial z^2} + k_\perp^2\right)\vec{A} = \frac{4\pi}{c}\left(\vec{J}_{nr} + \vec{J}_{fel}\right), \qquad (1)$$

where the source term has two distinct contributions: $\vec{J}_{nr}$, from the usual (nonresonant) cold beam response to the EM wave which is present in the absence of the wiggler, and a second term from the resonant FEL interaction. The resonant current J_{fel} is produced by the ponderomotive force of the EM wave beating with the magnetic field of the wiggler.[15] The beam is bunched in the ponderomotive wave, and the wiggling bunches produce the current which syncronously drives the EM wave. In the linear analysis (to which we restrict ourselves in this paper), this results in an exponentially growing instability. Since the parameters of the electron beam can be time-dependent, this can potentially lead to frequency-changing phenomena. The FEL is subject to frequency shifts when the driving terms $\vec{J}_{nr}$ and $\vec{J}_{fel}$ are time-dependent.

It is instructive to briefly summarize frequency shifting in passive media, such as occurs when radiation propagates through a moving inhomogeneous medium[16] with no FEL interaction. The wave equation, when used together with the canonical momentum conservation, becomes:

$$\left(\frac{1}{c^2}\frac{\partial^2}{\partial t^2} - \frac{\partial^2}{\partial z^2} + k_\perp^2\right)\vec{a} = -\frac{\omega_p^2(z,t)}{c^2}\vec{a}, \qquad (2)$$

where we have introduced the normalized vector potential of the radiation field $a = eA/mc^2$, e is the electron charge, m is the electron mass and c is the speed of light in vacuum. It is convenient to transform to the set of variables

$$s = t - \frac{z}{v_g}$$

$$z = z, \qquad (3)$$

where s is the distance from the head of the pulse, which propagates with group velocity v_g.

Using the eikonal approximation, which in our notation requires that variations in z are much slower than in s, results in:

$$\frac{\partial a(s,z)}{\partial z} = -\frac{-i\omega_p^2(s,z)v_g}{2\omega c^2}a(s,z). \qquad (4)$$

---

[14] M.E. Conde, C.J. Taylor, and G. Bekefi, submitted to *Phys. Fluids.*

[15] C.W. Roberson and P. Sprangle, *Phys. Fluids B* 1: 3 (1989).

[16] M. Lampe, E. Ott, and J.H. Walker, *Phys. Fluids* 21: 42 (1978); E. Esarey, A. Ting, and P. Sprangle, *Phys. Rev. A* 42: 3526 (1990).

While it is straightforward to integrate equation 4 by quadratures, further insight can be obtained by assuming that the density gradient is moving with constant velocity, v_b. Here, for a prescribed density profile $\omega_p^2(t - z/v_b)$,

$$a(s,z) = a(s,0)\exp(-i\Phi(s,z)), \tag{5}$$

and the frequency change, $\delta\omega = \partial\Phi/\partial s$, is now given by

$$\delta\omega(s,z) = \frac{\beta_b\beta_g}{2\omega(1-\beta_b/\beta_g)} \times \left[\omega_p^2(s) - \omega_p^2\left(s - \frac{z(1-\beta_b/\beta_g)}{v_b}\right)\right]. \tag{6}$$

It is instructive to analyze this equation in two limits. First, expanding the term $\omega_p^2\left(s - \frac{z(1-\beta_b/\beta_g)}{v_b}\right)$ in equation 6 results in an expression for the frequency change of a pulse that has propagated a distance z with the moving plasma:

$$\delta\omega(s,z) = \beta_g \frac{1}{\omega} z \frac{\partial\omega_p^2}{\partial(cs)}. \tag{7}$$

This expression is well behaved for $v_g = v_b$, and our subsequent analysis of the FEL amplifier will be carried out under this "zero slippage" assumption. Secondly, the opposite limit, that of a step profile electron beam, where finite slippage generates the frequency shift, can also be recovered from equation 6. Radiation starts inside the electron beam and eventually slips out of the beam, because $v_g > v_b$, is frequency upshifted by

$$\delta\omega = \frac{\beta_b\beta_g}{1-\beta_b/\beta_g}\frac{\omega_p^2}{2\omega}. \tag{8}$$

This effect is important in understanding the spectral characteristics of FEL oscillators.

Unfortunately, when the FEL interaction is included, the differential equation for the vector-potential is no longer first-order, and a simple integration, similar to the one above, is no longer possible.

We now restrict our analysis to the "zero slippage" approximation, which neglects the difference between group velocity of radiation and the velocity of an electron beam. This is reasonable for many microwave FELs which have long pulse-lengths, moderately relativistic energies and a reduction of the group velocity in the waveguide. For instance, in a recent studies of a Raman FEL,[17] the slippage parameter

$$S = \frac{L_{slip}}{L_{beam}} \tag{9}$$

is less than 5 percent. The FEL equations, which have temporal and spatial derivatives in the field equation, then become ordinary differential equations.

As is well known, a FEL with a helical wiggler and axial magnetic field, can be described, in the coordinates of equation 3, by

$$\frac{\partial\gamma(z,s)}{\partial z} = iC\frac{\beta_\perp}{2\beta_\parallel}a(z,s)\exp(i\theta) - i\frac{\omega_p^2(s)p_1^2}{c^2(k_z+k_w)}\exp(i\theta)<\exp(-i\theta)> \tag{10}$$

$$\frac{\partial\theta(z,s)}{\partial z} = k_z + k_w - \omega/v_\parallel \tag{11}$$

$$\frac{\partial a}{\partial z} + iF\frac{\omega_p^2(s)}{2\gamma\omega v_b}\frac{\omega - k_z v_b}{\omega - k_z v_b - \Omega_0/\gamma}a = 2\pi iC\frac{I(s)}{I_A}<\frac{\beta_\perp}{\beta_\parallel}\exp(-i\theta)>, \tag{12}$$

where $v_\parallel = \beta_\parallel c$ is the longitudinal electron velocity, $\theta = (k_z + k_w)z\omega t$- the slow varying ponderomotive phase, v_b is the unperturbed beam velocity, γ is the beam relativistic factor, $\Omega_0 = eB_0/mc$ is the cyclotron frequency due to the axial field B_0, F is a dimensionless filling factor, C is a geometric factor which depends on the waveguide and mode. The factor C is defined in Wurtele, Chu and Fajans

[17] M.E. Conde, C.J. Taylor, and G. Bekefi, submitted to *Phys. Fluids.*

(1990)[18] and roughly equals the inverse of the waveguide radius. A nonresonant beam-loading term, which is not present in earlier work,[18] has been included in equation 12. Equations 10-12 were linearized[18] with the approximation that force bunching and wave perturbation of the equilibrium orbits is negligible. The dispersion relation thereby obtained (including the beam-loading term) can be written

$$\left(\Gamma + F\frac{\omega_p^2(s)}{2\gamma\omega v_b}\frac{\omega - k_z v_b}{\omega - k_z v_b - \Omega_0/\gamma}\right)\times$$

$$\left((\Gamma + \Delta K)^2 - \frac{1}{\beta_{\|0}}\frac{\partial\beta_{\|0}}{\partial\gamma}\frac{p_\perp^2\omega_p^2}{c^2}\right)$$

$$= -\frac{\pi C^2\beta_{\perp 0}^2 I\omega}{\beta_{\|0}^4 c I_A}\frac{\partial\beta_{\|0}}{\partial\gamma} \qquad (13)$$

Equation 13 can be solved explicitly for the real part of Γ, the s derivative of which is easily related to the frequency shift. Frequency shifts are seen to occur because of two distinct mechanisms: the usual cold beam dielectric shift (from the beam density) and the coupling to the slow space-charge wave, which is due to the FEL interaction. The beam dielectric shift is physically equivalent to that of a cold plasma and is extensively described in the literature,[19] the FEL term, which has time-dependence from changes in beam voltage and current, has not been analyzed until now. Numerical evalution of this expression for the frequency shift from physically realizable pulse forms for the voltage and current is in agreement with the observed shifts in reference 12.

Further investigations to determine the effect of frequency shift phenomena on the performance of FEL user facilities and power sources for high gradient structures are ongoing.

This work was supported by the Air Force Office of Scientific Research, Department of Energy, National Science Foundation, and Lawrence Livermore National Laboratories. We thank Paul Woskov for lending us the frequency filter bank.

1.2 Plasma Wave Interactions—RF Heating And Current Generation

1.2.1 Introduction

Sponsors

Lawrence Livermore National Laboratories
Subcontract B-160456
National Aeronautics and Space Administration
Grant NAGW-2048
National Science Foundation
Grant ECS-88-22475
U.S. Department of Energy
Grant DE-FG02-91-ER-54109

Project Staff

Professor Abraham Bers, Dr. Abhay K. Ram, Dr. Carson C. Chow, Dr. Vladimir Fuchs, Michael C. Moldoveanu, Steven D. Schultz, Luigi Vacca

The work of this research group is concerned with studies on the electrodynamics of plasmas. Attention is directed toward understanding the nonlinear dynamics of plasmas driven by high-frequency electromagnetic fields (as in RF heating and current drive of magnetically confined plasmas, or in laser-plasma interactions) and the generation and propagation of unstable radiations from laser-plasma interactions and anisotropic electron distributions in space and astrophysical plasmas.

In the following we report on two studies of chaotic dynamics: the first in stimulated Brillouin scattering with particular application to optical fibers and the second in plasma ion-cyclotron orbits driven by electrostatic wave fields. The third report is on our progress in modeling and understanding of the observed current drive efficiency enhancement in the Joint European Torus (JET) through the synergistic use of ion-cyclotron range of frequency (ICRF) waves with lower-hybrid current drive (LHCD). The last report describes our recent study of the double stream cyclotron maser amplifier.

[18] J.S. Wurtele, R. Chu, and J. Fajans, *Phys. Fluids B* 2: 1626 (1990).

[19] E. Esarey, A. Ting, and P. Sprangle, *Phys. Rev. A* 42: 3526 (1990).

1.2.2 Chaotic Stimulated Brillouin Scattering (SBS) in an Optical Fiber

Sponsors

Lawrence Livermore National Laboratories
Subcontract B160456
National Science Foundation
Grant ECS-88-22475

As part of our studies on chaotic wave dynamics in spatially extended media, we have considered in some detail the SBS three-wave-interaction (3WI).

The dynamics of stimulated Brillouin scattering in a homogeneous medium of finite extent has captured considerable interest both in laser-plasma interactions[20] and optical fibers.[21] Nonstationary and chaotic behavior had been previously reported in SBS with external feedback such as reflection at the boundaries[22] or with models involving more than one pump.[23] Harrison et al.[24] have observed chaotic SBS experimentally in an optical fiber without feedback. Gaeta and Boyd[25] have performed similar experiments and obtained similar results. However, these scientist propose that the experimentally observed aperiodic behavior is due to amplification of noise.

We have shown[26] that with the addition of resonance detuning and without feedback, the spatiotemporal 3WI modeling SBS can be chaotic in a restricted parameter regime. The model we propose appears to be one of the simplest SBS models exhibiting chaos in spatially extended media. We utilize the nonlinear 3WI equations[27] in one dimension and time for the fields of the waves involved, including resonance detuning (δ).

In a typical experiment with fused silica optical fibers and a single-mode argon-ion laser operating at λ=514.5 nm, the parameters are: index of refraction n=1.46; acoustic velocity $c_a = 5.96 \times 10^3\ ms^{-1}$; acoustic damping rate $\gamma_a \simeq 270$ MHz; nonlinear coupling constant $K \simeq 66\ ms^{-1}V^{-1}$; and ratio of laser (or Stokes) to acoustic damping rate $\gamma_0/\gamma_a \simeq 10^{-3.28}$ Since the damping length of the acoustic wave (c_a/γ_a) is much smaller than the typical interaction length $\sqrt{c_a c/n}/Ka_0$ (x = 0), we can ignore the convective term in the acoustic equation. Also, the damping on the laser and Stokes em waves are weak and can be ignored. Length and time scales can be rescaled with $\gamma_a t \rightarrow t$, $x\gamma_a(n/c) \rightarrow x$, $\Delta = \delta/\gamma_a$, and the wave amplitudes can be rescaled with $E_0 = a_0K/\gamma_a$, $E_s = a_sK/\gamma_a$, $E_a = (a_aK/\gamma_a)\exp(-i\Delta t)$. The SBS equations become

$$\partial_t E_0 + \partial_x E_0 = -E_s E_a, \tag{1}$$

$$\partial_t E_s - \partial_x E_s = E_0 E_a^*, \tag{2}$$

$$\partial_t E_a + (1 + i\Delta)E_a = E_0 E_s^*, \tag{3}$$

with the boundary conditions $E_0(x = 0,t) = a_0(x = 0)K/\gamma_a \equiv A$, $E_s(x = L,t) = \varepsilon$. The scattered wave is assumed to grow from a small amplitude (noise) ε at the right boundary. The laser wave E_0 is referred to as the pump, the scattered light wave E_s is often called the Stokes wave. In terms of a

---

[20] C.J. Randall and J.R. Albritton, *Phys. Rev. Lett.* 52: 1887 (1984); K. Sauer and K. Baumgärtel, *Phys. Rev. Lett.* 52: 101 (1984); R. Blaha, E.W. Laedke, A.M. Rubenchik, and K.H. Spatschek, *Europhys. Lett.* 7: 237 (1988); S. Hüller, P. Mulser, and A.M. Rubenchik, *Phys. Fluids B* 3: 3339 (1991).

[21] D. Cotter, *J. Opt. Commun.* 4: 10 (1983); I. Bar-Joseph, A.A. Friesem, E. Lichtman, and R.G. Waarts, *J. Opt. Soc. Am. B* 2: 1606 (1985); J. Coste and C. Montes, *Phys. Rev. A* 34: 3940 (1986); J. Botineau, C. Leycuras, C. Montes, and E. Picholle, *J. Opt. Soc. Am. B* 6: 300 (1989); R.G. Harrison, J.S. Uppal, A. Johnstone, and J.V. Moloney, *Phys. Rev. Lett.* 65: 167 (1990); A.L. Gaeta and R.W. Boyd, *Phys. Rev. A* 44: 3205 (1991).

[22] C.J. Randall and J.R. Albritton (1984); K. Sauer and K. Baumgärtel (1984); S. Hüller, et al. (1991).

[23] P. Narum, A.L. Gaeta, M.D. Skeldon, and R.W. Boyd, *J. Opt. Soc. Am. B* 5: 623 (1988); A.L. Gaeta, M.D. Skeldon, R.W. Boyd, P. Narum, *J. Opt. Soc. Am. B* 6: 1709 (1989).

[24] R.G. Harrison, et al. (1990).

[25] A.L. Gaeta and R.W. Boyd (1991).

[26] C.C. Chow, *Spatiotemporal Chaos in the Nonlinear Three Wave Interaction,* Ph.D. diss., Dept. of Physics, MIT, 1991; C.C. Chow and A. Bers, "Chaotic Stimulated Brillouin Scattering in a Finite Length Medium," *Phys. Rev. A,* forthcoming 1993.

[27] A. Bers, "Linear Waves and Instabilities," in *Plasma Physics—Les Houches* 1972, eds. C. DeWitt and J. Peyraud (New York: Gordon and Breach Publishers, 1975), pp. 113-215.

[28] D. Cotter (1983); R.G. Harrison, et al. (1990); A.L. Gaeta and R. Boyd (1991); D. Cotter, *Opt. Quantum Electron.* 19: 1 (1987).

typical optical fiber experiment, L=1 corresponds to 0.75 m, Δ=1 corresponds to 270 MHz, and A=ε=1 corresponds to 4 MVm^{-1}.

Equations (1) to (3) were numerically simulated.[29] The system has four free parameters A, Δ, ε, and L. However, a numerical survey of the parameter space indicated that a two-dimensional surface could capture the unfolding behavior. The Δ-A parameter plane for fixed L and ε was chosen. Figure 4 shows the numerically determined unfolding diagram in the Δ-A plane for L=40 and ε=0.0025. Parameters L and ε were chosen so that the bifurcation diagram in the Δ-A plane contained all the observed dynamics. For small Δ and A there is a stable fixed state. It becomes unstable through a Hopf bifurcation to a periodic state. Then there is a transition to quasi-periodicity and to chaos. Each region is discussed in detail in Chow's thesis and in a forthcoming publication.[30] There it is shown that the system described by equations (1) to (3) has one fixed state (figure 5) which is stable when there is no resonance detuning, $\Delta = 0$. For $\Delta \neq 0$, there is a phase twist over the distance, in both the pump (laser) and Stokes waves, which depends on both Δ and A. When the phase twist exceeds a certain threshold, the fixed state becomes unstable and Hopf-bifurcates to a periodic state (figure 6). For the chaotic regime (figure 7) to occur, the reflectivity must be high and the medium must be larger than the growth length of the Stokes wave. Note that the coherence length of the pump structures is on the order of the growth length of the Stokes wave. Thus the resulting chaos is low-dimensional and does not exhibit spatiotemporal chaos.[31]

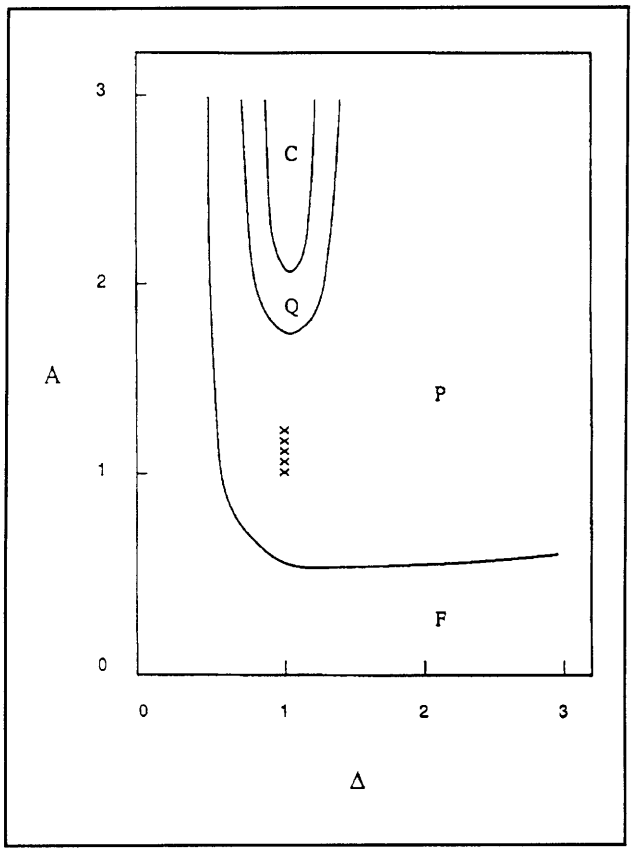

Figure 4. Bifurcation diagram in the Δ-A plane for L = 40 and ε= 0.0025. There are four different phases: F denotes the fixed state, P denotes the periodic orbit, Q denotes quasi-periodicity and C denotes chaos. The line of x's indicate a region of phase coexistence between a periodic and a quasi-periodic orbit.

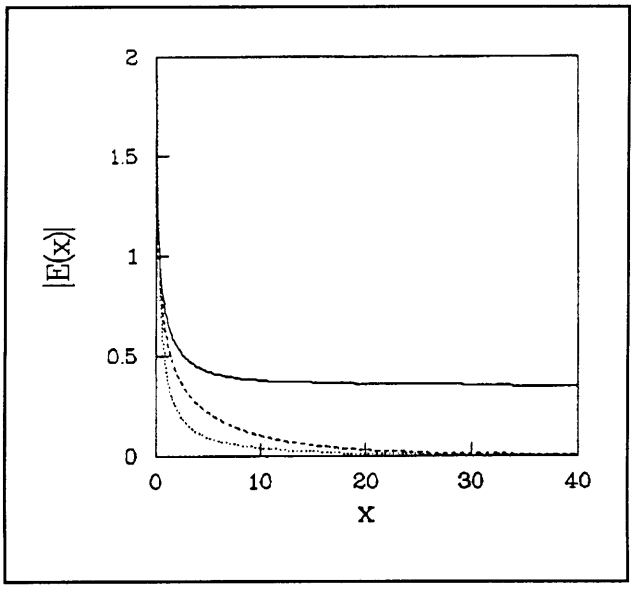

Figure 5. Fixed state spatial profiles of the pump (solid line), Stokes wave (dashed line) and acoustic wave (dotted line) for the parameters Δ = 0, A = 1.6, L = 20, ε = 0.0025.

[29] C.C. Chow, Ph.D. diss., Department of Physics, MIT, 1991.

[30] C.C. Chow, Ph.D. diss., Department of Physics, MIT, 1991; C.C. Chow and A. Bers, *Phys. Rev. A*, forthcoming 1993.

[31] C.C. Chow, Ph.D. diss., Dept. of Physics, MIT, 1991; C.C. Chow, A. Bers, and A.K. Ram, "Spatiotemporal Chaos in the Nonlinear Three Wave Interaction," *Phys. Rev. Lett.* 68: 3379 (1992).

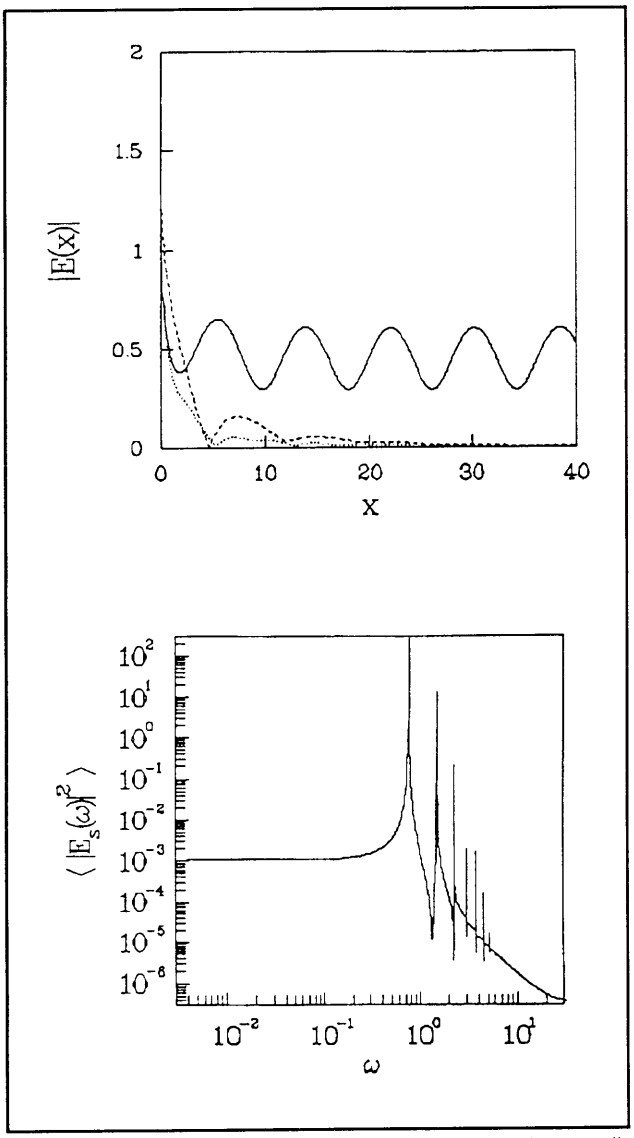

Figure 6. (a) Periodic state: Spatial profile of the amplitudes at a fixed time at (Δ = 1, A = 1). (b) Periodic state: Power spectrum of pump at (Δ = 1, A = 1).

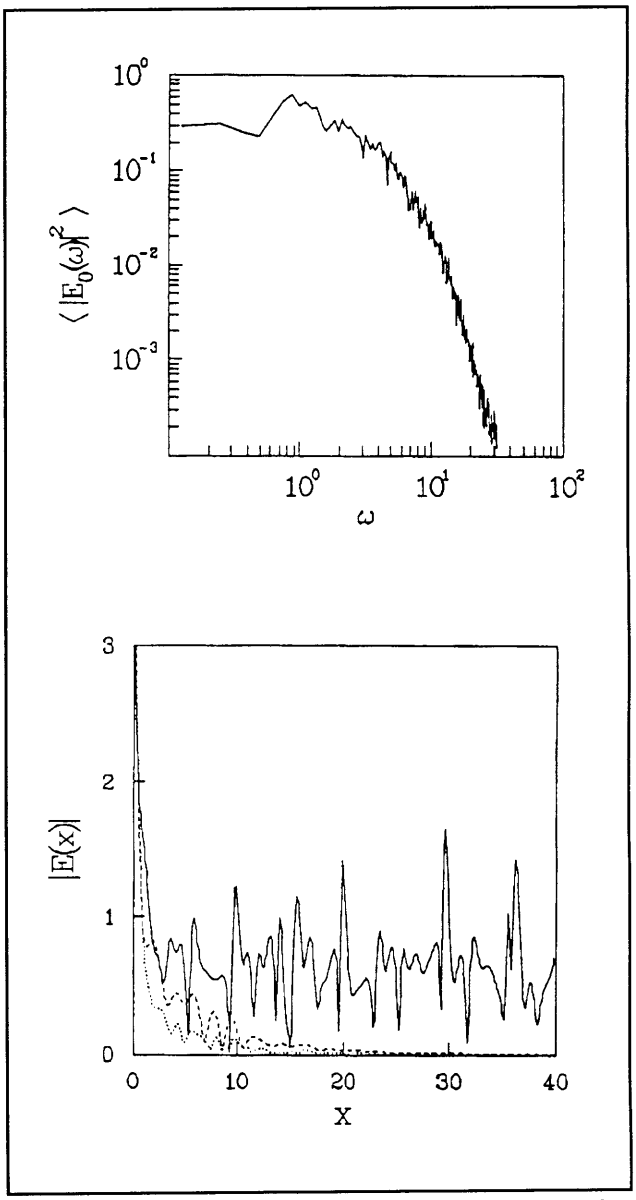

Figure 7. (a) Chaotic state: Spatial profile at (Δ = 1, A = 5). (b) Chaotic state: Power spectrum of the pump at (Δ = 1, A = 5).

1.2.3 Chaotic Webs in Ion-orbit Chaos Induced by Waves

Sponsors

National Aeronautics and Space Administration
Grant NAGW-2048
National Science Foundation
Grant ECS 88-22475
U.S. Department of Energy
Contract DE-FG02-91-ER-54109

The motion of a charged particle in a steady magnetic field and acted upon by an electrostatic wave, propagating in a direction perpendicular to the magnetic field, can be written as:

$$\ddot{x} + \omega_c^2 x = \frac{eE_o}{m} \sin(kx - \omega t) \qquad (1)$$

where e is the charge of a particle of mass m, ω_c is the cyclotron frequency of the particle in the constant magnetic field, E_o is the amplitude of the electrostatic wave with wavenumber k and frequency ω. By using the normalized variables $\tau = \omega t$, $q = kx$, $p = k\dot{x}/\omega$, and $\Omega = \omega_c/\omega$, the Hamiltonian corresponding to the above equation of motion can be written as:

$$H(q,p,\tau) = \frac{p^2}{2} + \frac{\Omega^2}{2} q^2 + \varepsilon \cos(q - \tau) \qquad (2)$$

where $\varepsilon = eE_0k/(m\omega^2)$ is the normalized amplitude of the electric field. By defining the action-angle, (I,ψ), coordinates:

$$I = \frac{\Omega}{2}\left(q^2 + \frac{p^2}{\Omega^2}\right)$$

$$\psi = \tan^{-1}\left(\frac{\Omega q}{p}\right)$$

the above Hamiltonian can be transformed to:

$$H = \Omega I + \varepsilon \cos\left(\sqrt{\frac{2I}{\Omega}}\sin\psi - \tau\right)$$

$$= \Omega I + \varepsilon \sum_{-\infty}^{\infty} J_n\left(\sqrt{\frac{2I}{\Omega}}\right)\cos(n\psi - \tau) \qquad (3)$$

This Hamiltonian has been examined in a variety of regimes by several authors. The case when $1/\Omega \neq$ integer (the non-resonant case) has been examined in detail by Karney.[32] There it was found, using an analysis similar to the Chirikov resonance overlap criterion, that the motion of the ions became chaotic for amplitudes $\varepsilon > \Omega^{4/3}$; the chaotic region in *p*-space being limited from below by trapping condition: $p \gtrsim 1 - \sqrt{\varepsilon}$, and from above by $p \lesssim (10n^2\varepsilon^2/\Omega)^{1/3}$ (where *n* is the closest integer to $1/\Omega$). From these conditions, it is clear that the threshold amplitude goes down as the frequency of the wave becomes much higher than the cyclotron frequency and, correspondingly, the extent of the region in *p*-space becomes wider as the amplitude is increased.

For $1/\Omega = n$, an integer (i.e., the wave frequency is an integer multiple of the particle cyclotron frequency; this will be referred to as the resonant case), the motion of the charged particle was first examined by Fukuyama et al.[33] and later by Chernikov, et al. and Zaslavsky.[34] The former found conditions for attaining wide-spread chaos, when $p \gg n$, using the Chirikov resonance overlap criterion, while the latter showed the existence of chaotic "webs." The importance of the web is twofold: first, the chaotic web has no amplitude threshold condition, although the chaotic region is very thin at low amplitudes; second, the chaotic web exists over all phase space extending down to zero energies. These characteristics could obviously have important new applications for such wave induced chaos. The crucial problem is to determine the parameter regime for which the web is sufficiently thick to have a significant part of phase space chaotic, and, of course, the relationship between, and transition from, web chaos to the Chirikov-type global, but limited range, chaos which we already know for this problem. Below, we present some sample calculations illustrating the intriguing aspects of web chaos.

In the resonant case all the particle orbits are confined to islands. For small amplitudes, ε, the islands lie between the zeros of the Bessel function $J_n(\sqrt{2In})$, where $1/\Omega = n$. The separatrices of these islands are connected in a web structure, and a particle started on this web will diffuse along the web (figure 8). As ε is increased, the web widens occupying a larger fraction of the phase space. This increases the region of phase space for which the motion of the particle is chaotic (figure 9). Since the web is connected over the entire range of *I*, a particle starting on the web can, in principle, diffuse over the whole range of *I*. Note, however, that the lower energy region tends toward global chaos, while the web extension to higher energies remains rather thin.

In the slightly nonresonant case, and for small ε, there appear untrapped particle orbits which separate (in *I*) the islands mentioned above (figure 10). Even though the islands occupy most of the phase space, the web structure does not connect all the islands as in the resonant case. However, there exists a periodic web structure which is separated in *I* by untrapped particle orbits. The particle orbits can diffuse along this web structure bounded in *I*. Increasing ε does not restore the web structure of the resonant case. However, it does lead to local regions of chaotic motion which are formed by the widening of the webs (figures 11a and 11b).

As the wave frequency and the particle cyclotron frequency get farther off resonance, for small ε a larger region of phase space is occupied by untrapped particle orbits (figure 11a), until eventually, when the frequencies are sufficiently nonresonant, the entire phase space is occupied by

---

[32] C.F.F. Karney and A. Bers, *Phys. Rev. Lett.* 39: 550 (1977); C.F.F. Karney, *Phys. Fluids* 21: 1584 (1978).

[33] A. Fukuyama, H. Momota, R. Itatini, and T. Takizuka, *Phys. Rev. Lett.* 38: 701 (1977).

[34] A.A. Chernikov, M. Ya. Natenzon, B.A. Petrovichev, R.Z. Sagdeev, and G.M. Zaslavsky, *Phys. Lett. A* 129: 377 (1988); G.M. Zaslavsky, *Chaos* 1: 1 (1991).

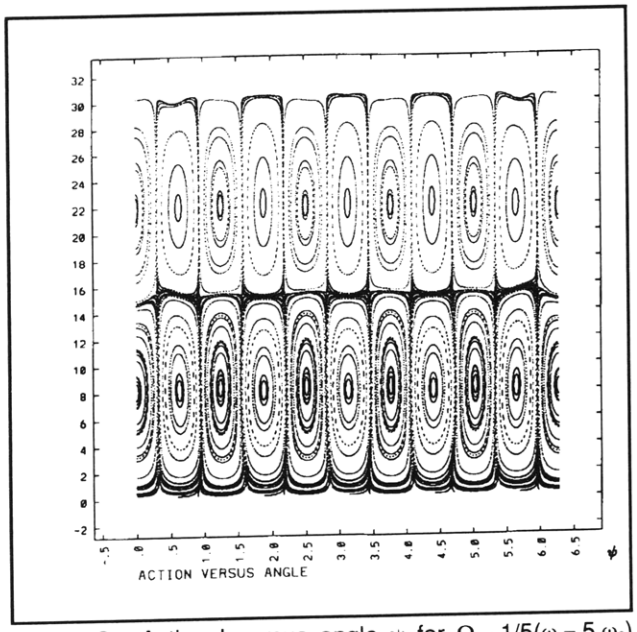

Figure 8. Action I versus angle ψ for $\Omega = 1/5(\omega = 5\ \omega_0)$ and $\varepsilon = 10^{-2}$.

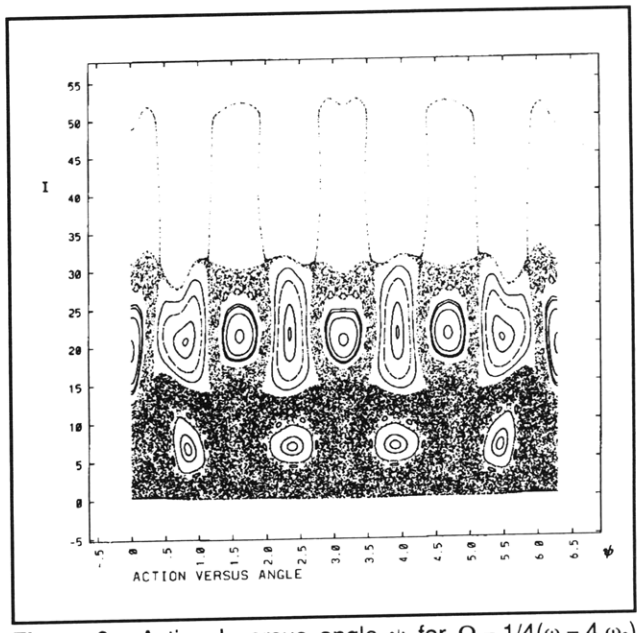

Figure 9. Action I versus angle ψ for $\Omega = 1/4(\omega = 4\ \omega_0)$ and $\varepsilon = 10^{-1}$.

untrapped particle orbits. In this case, as ε is increased, there again appear islands in phase space where the particle orbits are trapped.

We are presently examining these puzzling features of web chaos, a new type of chaos, and its relation to the more commonly encountered Chirikov resonance overlap chaos.

1.2.4 Lower Hybrid Current Drive in the Presence of Waves in the Ion Cyclotron Range of Frequencies

Sponsor

U.S. Department of Energy
Contract DE-FG02-91-ER-54109

In a set of recent experiments on the Joint European Tokamak (JET),[35] it was observed that the lower hybrid (LH) current drive (CD) efficiency was significantly enhanced when the current driving lower hybrid waves (LHW) were launched in the presence of waves in the ion cyclotron range of frequencies (ICRF). The experiments were performed in a deuterium plasma with a hydrogen minority; an asymmetric (current drive mode) LHW $k_\parallel$-spectrum and a symmetric (heating mode) ICRF $k_\parallel$-spectrum were applied externally. The experimental conditions for the enhancement in CD efficiency required that the ICRF antenna be in a monopole configuration and that the ion cyclotron and ion-ion hybrid resonance layers be located near the center of the plasma. In fact, if any of the these two conditions were not satisfied, no enhancement in the CD efficiency was observed.

The initial ICRF power is carried from the antenna into the center of the plasma by fast Alfvén waves (FAW). At the resonance layers located inside the plasma some of this power is mode converted to ion-Bernstein waves (IBW). These IBWs then propagate away from the plasma core. The mode conversion is most efficient for small $k_\parallel$'s ($k_\parallel$ is the component of the total wave vector along the toroidal magnetic field).

The FAWs can directly and indirectly heat the electrons. The direct heating is through electron Landau damping and transit time magnetic pumping. The indirect heating is by the slowing down of the energetic minority ion tails, generated by FAWs, on the electron distribution. This heating of electrons is known to lead to an enhancement in the LHCD efficiency and was first observed on the Japanese tokamak JT-60 (and, hence, known as the JT-60

[35] C. Gormezano, M. Brusanti, A. Ekedahl, P. Froissard, J. Jaquinot, and F. Rimini, *Proceedings of the IAEA Technical Meeting on Fast Wave Current in Reactor Scale Tokamaks (Synergy and Complementarity with LHCD and ECRH),* Arles, France, September 23-25, 1991, eds. D. Moreau, A. Bécoulet, and Y. Peysson, pp. 244-259.

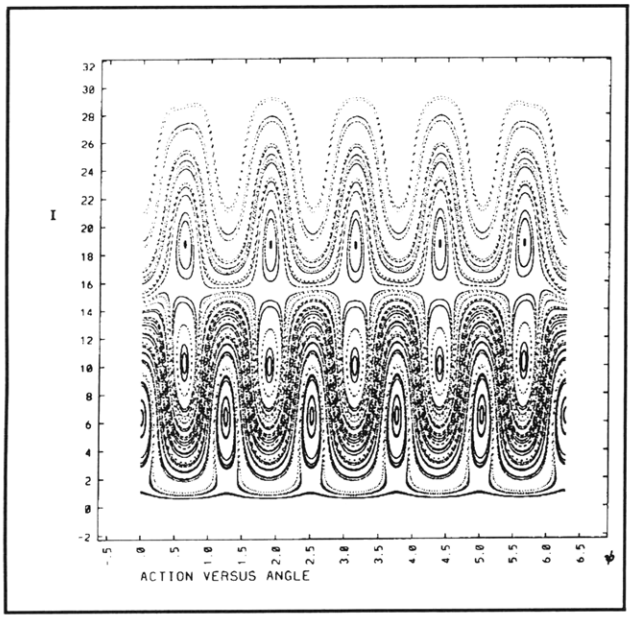

Figure 10. Action I versus angle ψ for $\Omega = 1/5.02(\omega = 5.02\ \omega_0)$ and $\varepsilon = 10^{-2}$.

effect).[36] The FAWs can also interact with the electron tail pulled out by the LHWs.

For the IBWs, the initial mode converted spectrum has parallel (to the toroidal magnetic field) phase velocities which are much larger than the parallel electron thermal velocity. Thus, the IBWs cannot, initially, interact with the electron distribution function unless it has a runaway tail. The IBW spectrum also cannot interact with the ion distribution function as the mode conversion point is sufficiently far away from the ion cyclotron resonance. However, as the IBWs propagate away from the mode conversion region, toroidal effects upshift the $|k'_{\parallel}|$'s so that eventually the IBW spectrum can interact with the LHCD electron distribution function.[37] The interaction is in the form of Landau damping. Thus, the IBWs can interact with the energetic electron tail pulled out by the LHWs.

Although several models have been proposed, the JT-60 effect remains largely unexplained. Since JET observed enhancements in the CD efficiency beyond those due to the JT-60 effect, we have concentrated our efforts toward understanding the direct interaction of the FAWs and IBWs with the

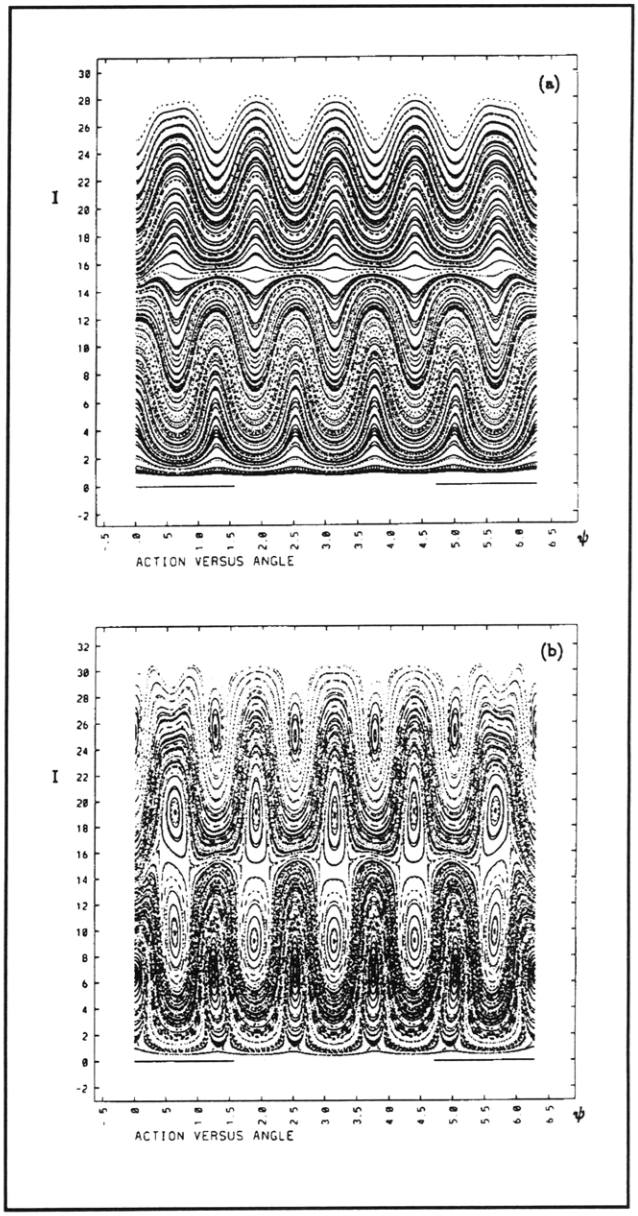

Figure 11. Action I versus angle ψ for $\Omega = 1/5.05(\omega = 5.05\ \omega_0)$: (a) $\varepsilon = 10^{-2}$; (b) $\varepsilon = 3 \times 10^{-2}$.

LH generated asymmetric electron distribution function. Toward this end, we have studied solutions of the relativistic Fokker-Planck equation describing the evolution of the electron distribution function, on a given flux surface, when acted upon by LHWs

36 T. Imai and JT-60 Team, IAEA, 13th International Conference on Plasma Physics & Contributions to Nuclear Fusion Research, Washington, D.C., October 1-6, 1990, paper CN-53/E-1-3.

37 A.K. Ram and A. Bers, "Propagation and Damping of Mode Converted Ion-Bernstein Waves in Toroidal Plasmas," *Phys. Fluids B* 3: 1059 (1991).

and either FAWs or IBWs.[38] The evolution of the flux surface averaged electron distribution function, in a uniform magnetic field and for wave frequencies ω below the electron cyclotron frequency ω_{ce}, is given by:

$$\frac{\partial}{\partial t} f_o = \frac{\partial}{\partial p_\parallel} D^{LHW} \frac{\partial}{\partial p_\parallel} f_o + \frac{\partial}{\partial p_\parallel} D^{FAW/IBW} \frac{\partial}{\partial p_\parallel} f_o + \left(\frac{\partial}{\partial t} f_o \right)_{collisional}$$

where the *D*s are the appropriate quasilinear diffusion coefficients and $p_\parallel$ is the component of the electron momentum along the total magnetic field. Following the usual procedures,[39] we express the quasilinear diffusion coefficients in the following forms:

$$D^{LHW} = \pi e^2 |E_{kz}|^2 \delta\left(k_\parallel - \frac{\omega}{v_\parallel}\right) D_o^{LHW}$$

$$D^{FAW/IBW} = \pi e^2 |E_{ky}|^2 \delta\left(k_\parallel - \frac{\omega}{v_\parallel}\right) D_o^{FAW/IBW} \qquad (1)$$

where

$$D_o^{LHW} = \frac{1}{|v_\parallel|} \left[\left\{ J_0 - \frac{v_\perp}{v_\parallel} J_1 Im\left(\frac{E_{ky}}{E_{kz}} \right) \right\}^2 + \left\{ \frac{v_\perp}{v_\parallel} J_1 Re\left(\frac{E_{ky}}{E_{kz}} \right) \right\}^2 \right]$$

$$D_o^{FAW/IBW} = \frac{1}{|v_\parallel|} \left[\left\{ \frac{v_\perp}{v_\parallel} J_1 + J_0 Im\left(\frac{E_{kz}}{E_{ky}} \right) \right\}^2 + \left\{ J_0 Re\left(\frac{E_{kz}}{E_{ky}} \right) \right\}^2 \right] \qquad (2)$$

e is the electron charge, *v*'s are the velocities (with the component perpendicular to the magnetic field having the subscript $\perp$), E_k's are the appropriate components of the Fourier transformed electric field spectrum, and the argument of the Bessel functions, J_0 and J_1, is $(k_\perp v_\perp)/\omega_{ce}$. The purpose of expressing the diffusion coefficients in different forms for the LHWs and the FAW/IBWs is that the factor multiplying D_o in equation (1) is essentially determined by the input power spectrum. Meanwhile, D_o in equation (2) depends only on the local plasma properties and polarizations of the fields. For typical JET-type parameters, we find that $D_o^{FAW}/D_o^{LHW} \approx (k_\perp \rho_e)^2$ where ρ_e is the electron Larmor radius. Then, from equation (1), one can see that the diffusion coefficient for the FAW will be small compared to the LHW diffusion coefficient for similar powers. Then, on the basis of this comparison between the FAW and LHW diffusion coefficients, one expects that the FAW should not have a significant effect on the LH generated electron tails. Indeed, numerical solutions of the Fokker-Planck equation confirm this fact.

Meanwhile, since there is no easy way to evaluate the electric field polarizations for the IBW, a similar type of analytical analysis comparing the IBW diffusion coefficient with the LHW diffusion coefficient is not practical. However, numerical evaluations

[38] A. Bers and A.K. Ram, "Lower Hybrid and Fast Wave Current Drive—Status of Theory," *Proceedings of the IAEA Technical Meeting on Fast Wave Current in Reactor Scale Tokamaks (Synergy and Complementarity with LHCD and ECRH),* Arles, France, September 23-25, 1991, eds. D. Moreau, A. Bécoulet, and Y. Peysson, pp. 2-34; Ram, A.K., A. Bers, V. Fuchs, R.W. Harvey, and M.G. McCoy. "Effects of Fast Alfvén Waves in Lower Hybrid Current Drive," *Proceedings of the Europhysics Topical Conference on RF Heating and Current Drive of Fusion Devices,* Brussels, Belgium, July 7-10, 1992, pp. 201-204; A.K. Ram, A. Bers, V. Fuchs, R.W. Harvey, and M.G. McCoy, "Current Drive by Lower Hybrid Waves in Presence of Fast Alfvén Waves," *Bull. Am. Phys. Soc.* 37(6): 1605 (1992); A.K. Ram, A. Bers, V. Fuchs, R.W. Harvey, and M.G. McCoy, "Effect of ICRF Waves on Lower Hybrid Current Drive," *Proceedings of the US-Japan Workshop on Non-Inductive Current Drive and Profile Control,* Princeton Plasma Physics Laboratory, 14-16, 1992.

[39] C.F. Kennel and F. Engelmann, *Phys. Fluids* 9: 2377 (1966); I. Lerche, *Phys. Fluids* 11: 1720 (1968).

show that the D^{IBW} is small compared to D^{LHW} but larger than D^{FAW}. Although the mode converted power to the IBW is smaller than the input power on the FAW, the electric field amplitude along the IBW increases by almost an order of magnitude as the IBWs propagate in a tokamak plasma. This increase is due to the IBWs group velocities slowing down as they propagate away from the mode conversion region. Numerical solutions of the Fokker-Planck equation then show that the IBWs can significantly affect the electron distribution function and, consequently, lead to an enhancement in the current drive efficiency.

Another important aspect of the IBWs is that they interact with electrons on the same flux surfaces on which the LHWs generate currents. It is well known that the LHCD generally occurs well off-axis in a tokamak. In experiments the ion resonances for ICRF waves are located near axis. So the FAW, which would interact with electrons near the ion resonances, is not interacting with the electrons on the flux surfaces where LHCD is generated. However, IBWs propagate away from the mode conversion region until there is sufficient enhancement in $|k_\parallel|$'s for the IBWs to interact with the electron distribution function. This interaction generally takes place well off-axis in the region where LHWs produce electron tails. This analysis is in general agreement with the experimental conditions required for an enhancement in the current drive efficiency.

1.2.5 Linear Analysis of the Double Stream Cyclotron Maser Instability

Sponsors

National Aeronautics and Space Administration
Grant NAGW-2048
National Science Foundation
Grant ECS-88-22475

The double stream cyclotron maser in which two copropagating electron beams with different beam velocities gyrate in a uniform axial magnetic field has been proposed as a source of millimeter wavelength radiation.[40] The interaction which leads to the radiation is between the slow cyclotron space charge of one beam and the fast cyclotron space charge of the other beam. This interaction leads to high frequency bunching of the electrons and subsequent radiation.

We have carried out a linear instability analysis of the linear, uniform medium dispersion relation describing the interaction of two such beams.[41] The dispersion relation describes the propagation of electrostatic waves, and, thus, is strictly valid for waves with phase velocities smaller than the speed of light. The analysis shows that electrostatic instabilities can be generated at frequencies lying near the doppler shifted electron cyclotron frequencies and also, approximately, half way between doppler shifted electron cyclotron frequencies. These instabilities exist for large $k_\parallel$ (the wave vector component along the magnetic field) with $\omega_r/k_\parallel < c$ (ω_r is the real part of the frequency and *c* is the speed of light). For low beam densities, typical of those under consideration, the calculations point out the distinct advantage of the two electron beam system. For a single beam of electrons, the slow cyclotron space charge wave near a harmonic of the electron cyclotron frequency does not interact with the fast space charge wave at a neighboring harmonic. The only instabilities in this case are near the electron cyclotron frequency and its harmonics, and for small $k_\parallel$ such that $\omega_r/k_\parallel > c$; this is the domain where the electrostatic approximation used to obtain the dispersion relation breaks down. Thus, the two beam system is important for generating emission at very high frequencies. In figure 12 we plot $(\omega_r - \bar{v}_\parallel k_\parallel)/\Omega$ (where $\bar{v}_\parallel$ is the average of the parallel velocities of the two beams and Ω is the average of the electron cyclotron frequency of the two beams) versus $ck_\parallel/\Omega$. The regions instability are easily identifiable.

We have extended our linear analysis to include parallel temperature spreads in the beams. It has been found that the growth rates of the instabilities decreases as the temperature goes up. However, for parameters relevant to experiments, the growth rate is not substantially reduced so that instabilities exist for high frequencies and short parallel wavelengths.

---

[40] G. Bekefi, *J. Appl. Phys.* 71: 4128 (1992).

[41] G. Bekefi, A.K. Ram, A. Bers, and C. Chen, *SPIE Proceedings of the 1992 OE LASE Conference,* Los Angeles, California, January 1992; A.K. Ram, C. Chen, A. Bers, W. Hu, and G. Bekefi, "Linear and Nonlinear Analysis of the Double Stream Cyclotron Maser," *Conference Record of the 19th IEEE International Conference on Plasma Science,* Tampa, Florida, 1-3 June 1992; A. Bers, A.K. Ram, and G. Bekefi, "Linear Analysis of the Double Stream Cyclotron Maser," *Bull. Am. Phys. Soc.* 37(6): 1536 (1992).

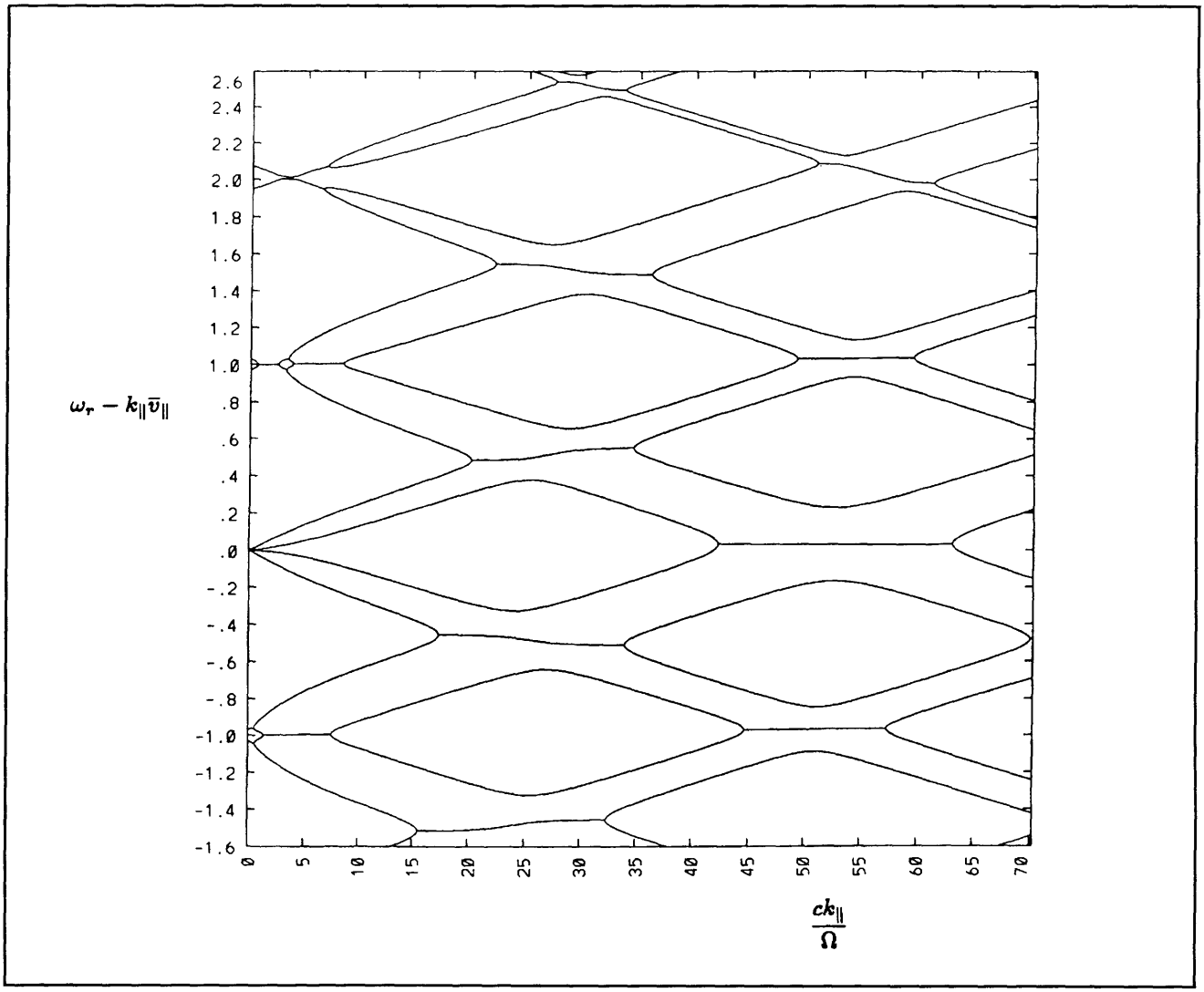

Figure 12. $\omega_r - \bar{v}_\parallel \frac{k_\parallel}{\Omega}$ versus $c\frac{k_\parallel}{\Omega}$ for two beams whose parallel velocities are separated by 0.038c.

1.2.6 Publications

Bekefi, G., A.K. Ram, A. Bers, and C. Chen. *SPIE Proceedings of the 1992 OE LASE Conference,* Los Angeles, California, January 1992.

Bers, A., and A.K. Ram. *Lower Hybrid and Fast Wave Current Drive—Status of Theory.* PFC/JA-92-3. Cambridge: MIT Plasma Fusion Center, January 1992.

Bers, A., and A.K. Ram. "Lower Hybrid and Fast Wave Current Drive—Status of Theory." *Proceedings of the IAEA Technical Meeting on Fast Wave Current in Reactor Scale Tokamaks* (Synergy and Complementarity with LHCD and ECRH), Arles, France, September 23-25, 1991. Eds. D. Moreau, A. Bécoulet, and Y. Peysson, pp. 2-4.

Bers, A., A.K. Ram, and G. Bekefi. "Linear Analysis of the Double Stream Cyclotron Maser." *Bull. Am. Phys. Soc.* 37(6): 1536 (1992).

Chow, C.C. *Spatiotemporal Chaos in the Nonlinear Three Wave Interaction.* Ph.D. diss., Department of Physics, MIT, 1991.

Chow, C.C., and A. Bers. *Chaotic Stimulated Brillouin Scattering in a Finite Length Medium.* PFC/JA-92-36. Cambridge: MIT Plasma Fusion Center, December 1992.

Chow, C.C., and A. Bers. "Chaotic Stimulated Brillouin Scattering in a Finite Length Medium," *Phys. Rev. A.* Forthcoming.

Chow, C.C., A. Bers, and A.K. Ram. "Spatiotemporal Chaos in the Langmuir Decay and its Implications on the Saturation of SRS." *Proceedings of the 22nd Anomalous Absorption Conference,* Lake Placid, New York, July 12-17, 1992.

Chow, C.C., A. Bers, and A.K. Ram. *Spatiotemporal Chaos in the Nonlinear Three Wave Interaction.* PFC/JA-92-2. Cambridge: MIT Plasma Fusion Center, January 1992.

Chow, C.C., A. Bers, and A.K. Ram. "Spatiotemporal Chaos in the Nonlinear Three-Wave Interaction." *Phys. Rev. Lett.* 68: 3379 (1992).

Chow, C.C., A. Bers, and A.K. Ram. "Spatiotemporal Chaos in Three Wave Interactions," Plasma Phys. Contr. Fusion, 34(13): 1945 (1992). Special Issue: Invited papers for the 1992 ICPP, Innsbruck, Austria, June 29-July 3, 1992.

Chow, C.C., A. Bers, and A.K. Ram. *Spatiotemporal Chaos in Three Wave Interactions.* PFC/JA-92-27. Cambridge: MIT Plasma Fusion Center, September 1992.

Chow, C.C., A. Bers, and A. K. Ram. "The Three Wave Interaction and Spatiotemporal Chaos." *Physics of Space Plasmas* (1991), SPI Conference Proceedings and Reprint Series, Number 11. Eds. T. Chang, G.B. Crew, and J.R. Jasperse. Cambridge: Scientific Publishers, 1992, pp. 179-195.

Chow, C.C., A. Bers, and A.K. Ram. *The Three Wave Interaction and Spatiotemporal Chaos.* PFC/JA-92-1. Cambridge: MIT Plasma Fusion Center, January 1992.

Chow, C.C., A.K. Ram, and A. Bers. "Spatiotemporal Chaos in the Nonlinear Three Wave Interaction," *Research Trends in Physics: Chaotic Dynamics and Transport in Fluids and Plasmas.* Eds. I. Prigogine, et al. New York: American Institute of Physics. Forthcoming.

Friedland, L., and A. Bers. *Hermitian Description of Interacting Inhomogeneous Electron Beams.* PFC/JA-92-15. Cambridge: MIT Plasma Fusion Center, April 1992.

Friedland, L., and A. Bers. "Hermitian Description of Interacting Inhomogeneous Electron Beams," *Phys. Fluids B (Plasma Physics)* 4: 1457 (1992).

Harvey, R.W., M.G. McCoy, A.K. Ram, A. Bers, and V. Fuchs. "Scaling of Lower Hybrid Current Drive with Temperature." *Proceedings of the Europhysics Topical Conference on RF Heating and Current Drive of Fusion Devices,* Brussels, Belgium, July 7-10, 1992, pp. 205-208.

Lashmore-Davies, C.N., A. Bers, and A.K. Ram. "Enhanced Electron Power Absorption of the Fast Wave in the Vicinity of the Two Ion Hybrid Resonance." *Bull. Am. Phys. Soc.* 37(6): 1583 (1992).

Ram, A.K., and A. Bers, "Comments on Absolute and Convective Instabilities." *Geophys. Res. Lett.* 19: 143 (1992).

Ram, A.K., A. Bers, V. Fuchs, R.W. Harvey, and M.G. McCoy. "Current Drive by Lower Hybrid Waves in Combination with Fast Alfvén Waves." *Proceedings of the International Sherwood Fusion Conference,* Santa Fe, New Mexico, April 6-8, 1992.

Ram, A.K., A. Bers, V. Fuchs, R.W. Harvey, and M.G. McCoy. "Current Drive by Lower Hybrid Waves in Presence of Fast Alfvén Waves." *Bull. Am. Phys. Soc.* 37(6): 1605 (1992).

Ram, A.K., A. Bers, V. Fuchs, R.W. Harvey, and M.G. McCoy. "Effects of Fast Alfvén Waves in Lower Hybrid Current Drive." *Proceedings of the Europhysics Topical Conference on RF Heating and Current Drive of Fusion Devices,* Brussels, Belgium, July 7-10, 1992, pp. 201-204.

Ram, A.K., A. Bers, V. Fuchs, R.W. Harvey, and M.G. McCoy. *Effects of Fast Alfvén Waves in Lower-Hybrid Current Drive.* PFC/JA-92-33. Cambridge: MIT Plasma Fusion Center, November 1992.

Ram, A.K., A. Bers, V. Fuchs, R.W. Harvey, and M.G. McCoy. "Effect of ICRF Waves on Lower Hybrid Current Drive." *Proceedings of the US-Japan Workshop on Non-Inductive Current Drive and Profile Control,* Princeton Plasma Physics Laboratory, 14-16, 1992.

Ram, A.K., C. Chen, A. Bers, W. Hu, and G. Bekefi. "Linear and Nonlinear Analysis of the Double Stream Cyclotron Maser." *Conference Record of the 19th IEEE International Conference on Plasma Science,* Tampa, Florida, June 1-3, 1992.

1.3 Physics of Thermonuclear Plasmas

Sponsor

U.S. Department of Energy
Contract DE-FGO2-91ER-54109

Project Staff

Professor Bruno Coppi, Neer R. Asherie, Dr. Paolo Detragiache, David S. Gloss, Dr. Cesar Meirelles-Filho, Dr. Stefano Migliuolo, Dr. Marco Nassi, Hana Ohkawa, Gregory E. Penn, Vladislav Portnoy, Caterina Riconda, Todd H. Rider, Dr. Barrett Rogers, Dr. Linda E. Sugiyama, Dr. Leonid E. Zakharov

As our primary activity in this research program, we study the theory of magnetically confined plasmas in regimes relevant to present-day advanced experiments and to future thermonuclear devices. In the future, these devices will probably ignite the plasma ("thermonuclear fuel") within toroidal magnetic confinement configurations and will involve either first generation fuels, a deuterium-tritium mixture (Ignitor, ITER), or more advanced fuels such as deuterium-deuterium or deuterium-helium mixtures (Candor).

The Ignitor-Ult machine is now in the early stages of construction in Europe. At MIT, the Alcator C-MOD experiment has recently begun operation. Alcator C-MOD combines the favorable features of an elongated plasma cross section with a high magnetic field to produce high plasma currents. This machine is in fact very similar to Megator, an experiment we proposed in the early 1970s as a logical continuation of the Alcator program.

Currently, our research program follows two major avenues. First, we are studying the basic physical processes of thermonuclear plasmas (equilibrium, stability, transport, etc.) as they apply to existing or near-term future systems. In this effort, we closely collaborate with our experimental colleagues and with theorists from other research groups (e.g., Columbia University, JET, Phillips Laboratory, Princeton University, University of Texas, Lawrence Livermore National Laboratories). This work also involves time-dependent simulations of plasma discharges in the Ignitor-Ult experiment. We focus particular attention on the evolution of spatial profiles of plasma current and temperature. Collaboration with our colleagues at the Italian laboratories, Energia Nucleare e Energie Alternative (E.N.E.A.), as well as inhouse code development by scientists "on loan" from Italy and the former Soviet Union, plays a major role in this endeavor.

Second, we explore advanced regimes of thermonuclear burning, including those employing low neutron yield fuels (D-^{3}He, and "catalyzed" D-D). We consider both the design of machines that will contain these very high temperature plasmas as well as the physics that govern their behavior. Below, we discuss some of the salient results of work completed or presently being carried out by members of our research group.

1.3.1 Theory of Reconnecting Modes in Collisionless Plasmas

We have investigated plasma processes capable of producing new magnetic field topologies (so-called magnetic reconnection) in collisionless, high temperature regimes.

In particular, we have developed a theory[42] of m = 1 modes based on a kinetic description of the plasma dynamics inside the reconnection layer of width δ_R about the $q(r = r_1) = 1$ resonant surface where the parallel electric field $E_\parallel \neq 0$. At high temperatures, two scale distances characterize the plasma dynamics: the collisionless skin depth $d_e = c/\omega_{pe} \propto n^{-1/2}$ and the ion sound Larmor radius $\rho_s = (T_e/m_i)^{1/2}/\Omega_{ci} \propto T_e^{1/2}/B$. Here $T_{e,i}$ are the electron and ion temperatures, and Ω_{ci} is the ion gyrofrequency. Typically, experiments operate in regimes where $\rho_s > d_e$. A third scale distance of the problem is given by $\lambda_H r_1$, where λ_H is the ideal-MHD stability parameter (a functional of the global equilibrium profiles). We have focused on the case of ideal-MHD marginal stability $\lambda_H = 0$. In this case, $\delta_R \sim \rho_s$ and the parallel current density $J_\parallel$ is confined to a sub-layer of width $\sim d_e$. By numerically solving the relevant mode equation, we find a mode growth rate $\gamma/\omega_A \approx (d_e/r_1)\,['1 + 1/(2\sqrt{\pi})\,(1+T_i/T_e)^{1/2}\rho_s/d_e]$ (ω_A is the shear Alfvén wave frequency) that can be quite fast, in particular for the parameters of the JET experiment when additional heating is used to enhance the plasma temperature.) In fact, we have proposed that the crash phase of the "sawtooth oscillations" in these experiments may be caused by the excitation of these modes.

At high temperatures, another effect that needs to be included in the analysis is that of the "drift" fre-

[42] B. Coppi and P. Detragiache, *Phys. Lett. A,* 168: 59 (1992); B. Coppi and P. Detragiache, RLE PTP-Report 92-9, MIT, submitted to *Ann. Phys.* (1992).

quencies $\omega_{*j} \propto T_j/B$ (j denotes the species: electrons or ions), related to the local equilibrium density (L_n) and temperature (L_{Tj}) gradient scale lengths, that is strongly stabilizing for $\omega_{*e} > \gamma$. Now, since $\omega_{*e}/\omega_A = \alpha_*(1 + L_n/L_T)(\rho_s/d_e)^2 d_e/r_o$, where $\alpha_* = (m_e/m_i)^{1/2} L_s/L_n$ and L_s is the magnetic shear length, ω_*-effects become dominant at large ρ_s/d_e. By numerically solving the relevant mode equation,[42] we have verified that, for realistic values of L_s/L_n, there is only a small interval in ρ_s/d_e in which an enhancement of the growth rate by high temperature effects can be achieved, with a further increase in temperature (i.e., in ρ_s/d_e) leading to a strong stabilization of the mode.

1.3.2 Linear and Nonlinear Kink-Tearing Modes

A linear, two fluid model of the collisionless reconnecting mode in tokamaks has also been formulated, leading to a stability condition, which is in qualitative agreement with experimental observations of sawtooth activity in contemporary, high temperature experiments. In contrast to the predictions of the ideal MHD m = 1 mode theory, the density and temperature gradients $n'(r_1)$, $T'_{e,i}(r_1)$ (associated with the so-called ω_*-effects[43]) play a stabilizing role in this condition while the magnetic shear $q'(r_1)$ is a destabilizing factor. Here, $q(r) = rB_\zeta/(RB_\theta)$ is the "safety factor", B_ζ and B_θ are the toroidal and poloidal magnetic fields, r and R are the minor and major plasma radii, and r_1 is the radius where $q(r_1) = 1$. An approximate form of this stability condition may be written as

$$0.04\mu^{1/6} \left| \frac{(T_e+T_i)\,|n'|\,R}{B_\zeta^2} \left[\frac{(T'_e + T'_i)n}{(T_e + T_i)n'} \right]^{1/3} \right|_{r=r_1}$$

$$> q'(r_1)r_1, \qquad \mu = \frac{m_i}{2m_p} \tag{1}$$

in terms of practical units: keV, 10^{13} cm^{-3}, Tesla, are used for $T_{e,i}$, n and B.

We have also considered the nonlinear evolution of the sawtooth crash in tokamaks. Specifically, our study addressed the early nonlinear stage of the crash, when the plasma central core displacement $\xi_0(t)$ is still small with respect to the radius $r = r_1$ but exceeds the characteristic width of the narrow layer in which the magnetic reconnection occurs. First, the helically symmetric magnetic geometry of the nonlinear reconnecting mode was determined by solving Waelbroeck's equations.[44]

Waelbroeck's equations are essentially approximate forms of the MHD equilibrium equation and the global flux conservation condition, which are valid when the crash time is slow compared to the relevant Alfvén time $\tau_A = 1/\omega_A$, but fast when compared to the resistive diffusion time. A typical result is plotted in figure 13, which shows a poloidal cross section of constant helical flux surfaces for a particular central core displacement. Combining this solution with the estimate of the reconnection layer width appropriate to current experiments, $\Delta \sim \rho_\tau = \sqrt{(T_e + T_i)/m_i}/\Omega_{ci}$, exponential growth of the mode was found with a rate $\gamma \approx q'(r_1)\rho_\tau\omega_A$. This result is also in good agreement[45] with experimental observations of the "fast" crash.

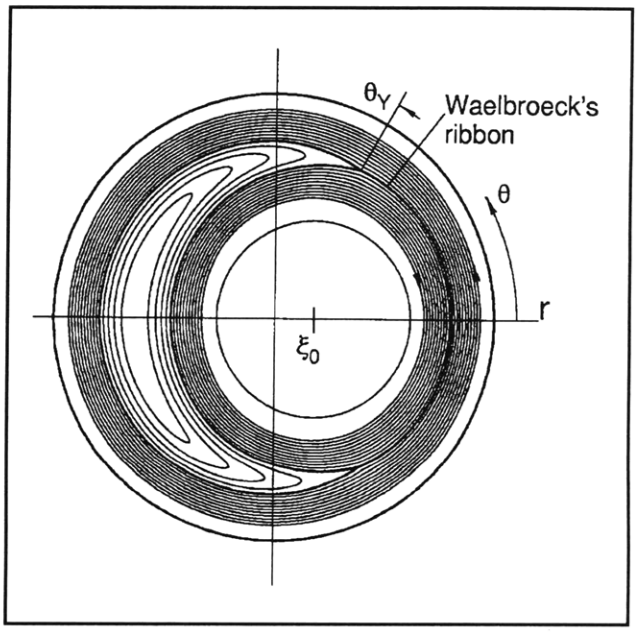

Figure 13. Magnetic configuration during the early nonlinear stage.

---

[43] G. Ara, B. Basu, B. Coppi, G. Laval, M.N. Rosenbluth, and B.V. Waddell, *N.Y. Ann. Phys.* 112: 443 (1978).

[44] F.L. Waelbroeck, *Phys. Fluids* B 1: 2372 (1989).

[45] L.E. Zakharov, B.N. Rogers, and S. Migliuolo, *Phys. Fluids* B 5, forthcoming.

1.3.3 Impurity Effects on Ion Temperature Gradient Microturbulence

The role played by impurities in influencing the linear stability properties of ion temperature gradient (ITG) modes has been considered with the intent to elucidate the role played by this turbulence in producing anomalous transport at the plasma edge. As is well-known, conventional gyro-Bohm transport models predict thermal diffusivities that scale as $T^{3/2}$, thereby becoming small in the outer plasma. (This is contrary to observed trends.)

The addition of one or more impurity (ion) species has one effect that may be termed beneficial in terms of transport: it leads to a dilution in the primary ion concentration ($n_i = n_e - Z_I n_I$, for a hydrogenic primary, where Z_I is the charge of the impurity ion) and, thus, a tendency to stabilize the standard ITG mode. Indeed, calculations[46] done in shearless slab geometry for collisionless plasmas indicate that the critical value of the ion temperature gradient parameter, $\eta_i \equiv d \ln T_i / d \ln n$ can increase by factors of 2-8 when an impurity species is present. The effect is stronger for higher ionization states and larger impurity mass.

This study was then carried out[47] for shaped plasmas in toroidal geometry, which is subject to the restriction that the mode frequency must be greater than the ion transit frequency. A collisionless, electrostatic, kinetic model was employed, and a considerable trend toward stabilization due to the impurity was found again. Of interest is the fact that three geometrical factors associated with the toroidal geometry and noncircular cross section of the plasma also contribute to smaller growth rates. The Shafranov shift has a strong stabilizing influence on the odd-parity mode and moderate stabilizing influence on the even-parity mode. Parity here refers to the property of the perturbed electrostatic potential when acted upon by a mirroring operator in the poloidal angle, $\theta \rightarrow -\theta$, where $\theta = 0$ corresponds to the outside of the torus farthest from the axis of symmetry). Ellipticity tends to strongly stabilize the even-parity mode and only moderately weaken the growth of the odd-parity mode. The situation is reversed for triangularity (odd-mode affected more strongly), which has a weaker stabilizing effect overall than ellipticity.

While impurities tend to stabilize the collisionless plasma, which is typically found in the center of high temperature present-day experiments, they can trigger their own brand of drift-wave type microinstability in collisional regimes (e.g., at the plasma edge). This type of mode is driven unstable by the temperature gradient of the primary ion species (like the ITG mode), but requires the presence of an impurity (preferably massive in comparison to the primary ions) and dissipation (e.g., a parallel thermal conductivity). It propagates in the electron diamagnetic direction for peaked impurity density profiles ($d \ln n_I / d \ln n_i \geq 1$). First discussed in the context of collisionless plasmas with reversed density profiles ($d \ln n_I / d \ln n_i < 0$),[48] its properties were elucidated later for collisional regimes.[49] Our recent analysis[50] has concentrated on properties in sheared slab geometries. This mode has been found to be robustly unstable, relatively impervious to magnetic shear, with an extended linear eigenfunction (more than 10 ion Larmor radii wide). Thus, it is a good candidate for the anomalous energy transport in the outer region of the plasma.

1.3.4 Emissions at the Harmonics of the Helium Gyro-Frequency

In recent experiments carried out with D-T plasmas in JET,[51] emissions were detected with a spectrum that showed distinct peaks at multiples ($l = 1 \rightarrow 8$) of the ^{4}He cyclotron frequency. An analysis[52] of the linear stability of collective modes indicates that these emissions are likely to arise because of the presence of an anisotropic (in velocity space) population of high-energy α-particles. These particles occur naturally as by-products of D-T thermonuclear fusion reactions. The relevant modes are shown to

---

46 S. Migliuolo, *Nucl. Fusion* 32: 1331 (1992).

47 S. Migliuolo, *Nucl. Fusion* 33: 3 (1993).

48 B. Coppi, H.P. Furth, M.N. Rosenbluth, and R.Z. Sagdeev, *Phys. Rev. Lett.* 17: 377 (1966).

49 B. Coppi, G. Rewoldt, and T. Schep, *Phys. Fluids* 19: 1144 (1976).

50 S. Migliuolo, *Phys. Lett. A,* forthcoming.

51 JET Team, *Nucl. Fusion* 32: 193 (1992).

52 B. Coppi, submitted to *Phys Lett. A*, 1992.

be spatially localized in a narrow layer centered on a surface near the edge of the plasma column. The position of this surface is consistent with that inferred from the value of the magnetic field that corresponds via the cyclotron frequency to the observed radiation. The width of the layer is compatible with the relatively narrow width of the peaks in the emitted spectrum. The outermost portion of the plasma is reached by α-particles that are trapped in orbits with relatively large values of $v_\perp/v_\parallel$. Work is underway[53] to determine the characteristics of the α-particle velocity space distribution function that are "optimal" for linear growth of these cyclotron harmonics, so that, in the future, emission spectra in other experiments can be used as a diagnostic tool. One additional issue being explored[54] is the effect of impurity ions on the emitted radiation: they may play an important role in determining some of the finer features in the observed spectrum.

1.3.5 Deuterium-Tritium Ignition Experiments with High Magnetic Fields

High magnetic field experiments have been designed to investigate deuterium-tritium fusion ignition conditions, on the basis of known experimental and theoretical understanding of plasma behavior. Our group has long maintained a strong effort in pioneering the practical use of such configurations. We have shown that the most advantageous and least expensive designs incorporate an interlocking set of characteristics: aspect ratio, relatively small size with significant vertical elongation, high toroidal and poloidal magnetic fields, large plasma currents, high plasma densities, good plasma purity, strong ohmic heating, good plasma and α-particle confinement, and robustness against ideal MHD and resistive plasma instabilities.[55] We have investigated the physical basis for these plasma properties, while also constructing the design and engineering solutions for attaining the necessary parameters in the Ignitor Ult machine[55] presently being built in Italy. Since ignition depends upon many spatially and temporally varying processes, many of our studies are based upon the numerical simulation of a free boundary plasma from the current ramp through ignition, using the MHD evolution and plasma flux surface transport code (TSC).[56]

The ignition of a 50:50 deuterium-tritium plasma requires a minimum value of the parameter $n_o\tau_E \approx 4 \times 10^{20}$ sec/m^3 in order to achieve ignition with $T_{eo} \approx T_{io} \leq 15$ keV, where n_o is the peak plasma (electron) density, T_{eo} the peak temperature, and τ_E the energy replacement time. Here ignition is defined as the point when the plasma heating due to fusion α-particles, P_α, equals the plasma thermal losses P_L. Relatively high values of the plasma density, $n_o \approx 10^{21}$ m^{-3}, then require only moderate values of τ_E, whose magnitude is less easy to predict with certainty. Both these values should be achievable, based on the favorable confinement properties of high density plasmas that have been demonstrated by a series of high field experiments, the Alcator A and C at MIT and the FT/FTU devices at Frascati, Italy. Experimentally, the maximum plasma density n_o that can be supported correlates with the ratio B_T/R_o, where B_T is the toroidal magnetic field at the center of the plasma column, at major radius $R = R_o$. On the basis of the Alcator C machine, where $n_o \approx 2 \times 10^{21}$ m^{-3} was achieved with $B_T \approx 12.5$ T and $R_o = 0.64$ m, and the TFTR machine at Princeton, where even larger ratios of n_oR_o/B_T were achieved, a configuration with $R_o \approx 1.3$m and $B_T \approx 13$ T should be able to sustain reliably densities of 10^{21} m^{-3}.

A strong toroidal magnetic field also supports a high poloidal field B_p and correspondingly large plasma current I_p. A significant vertical elongation, e.g., $\kappa \approx 1.8$, substantially increases the plasma current that can be carried for a given B_T and R. If the density correlates with the (volume) averaged toroidal current density, $< J_\phi >$, then experimental results suggest that somewhat less than 1 kA/cm^2 should offer considerable margin to attain the desired peak density $n_o \approx 10^{21}$ m^{-3}. High values of B_p produce a strong rate of ohmic heating, while large currents I_p tightly confine the fast α-particles produced by the fusion reactions, so that they deposit their energy in the center of the plasma. The degradation of the plasma energy confinement that is commonly observed when injected (nonohmic) heating is applied, is reduced at higher plasma current. In addition, the poloidal plasma beta β_p can be kept small at ignition, to improve the

---

53 B. Coppi and N. Asherie, *Bull. Am. Phys. Soc.* 37: 1475 (1992).

54 N. Asherie, in preparation (1993).

55 B. Coppi, M. Nassi, and L.E. Sugiyama, *Physica Scripta* 45: 112 (1992).

56 S.C. Jardin, N. Pomphrey, and J. Delucia, *J. Comp. Phys.* 66: 481 (1986).

plasma stability, and, in particular, to stabilize the ideal MHD modes with mode numbers m = 1, n = 1 that are associated with sawtooth oscillations. Large plasma density combined with good ohmic heating allows ignition at low plasma temperatures. This reduces the fusion power, and therefore the thermal wall loads. The low beta increases the overall margin of plasma stability.

The plasma purity has been shown to improve with increasing plasma density, that is, the effective charge $Z_{eff} = \sum n_i Z_i^2 / n_e$ decreases monotonically with n_e in an extensive series of experiments starting with the Alcator A. The major effect of impurities is to dilute the concentration of fusing nuclei, while a secondary effect is the increase of power loss due to bremsstrahlung radiation. If auxiliary heating is not used, Z_{eff} cannot exceed about 1.6 for D-T ignition in the Ignitor, as indicated by our analyses.

Relatively high plasma edge densities also help to confine impurities to the scrape off layer, where the induced radiation helps to distribute the thermal wall loading more uniformly over the plasma chamber surface. The low ignition temperatures associated with high density further help to keep the plasma clean by reducing the thermal wall loading that result in sputtering.

Peaked plasma density profiles should be maintained by external means such as pellet injectors if necessary. Peaked profiles maintain stability to ion temperature gradient modes that enhance the ion thermal transport. Since the neoclassical (Ware) inward particle pinch is relatively strong in a tight aspect ratio, high field configuration and an anomalous inflow are also present. Therefore, pellets that penetrate partway into the plasma can be successfully used to raise the plasma density and produce peaked profiles near ignition.

Plasma configurations such as X-points that concentrate the thermal (particle) heat flux on localized areas of the vessel wall limit the amount of fusion power that can be handled. In addition, an even more limited plasma current can be sustained. However, X-points and detached plasmas can be obtained with relatively little sacrifice in the plasma and magnet parameters. By creating the conditions known to produce "H-mode" operation, X-points and detached plasmas may prove desirable in limiting degradation of the plasma confinement caused by nonohmic heating.

Divertors represent a more severe compromise, since they alter the design of the plasma chamber and the toroidal magnet. The major radius must be increased to accommodate a reliable divertor, reducing the ratio B_T/R and therefore the maximum plasma density. The magnetic fields are also reduced, lowering the plasma current and the ohmic heating, and increasing β. A large injected heating system becomes necessary to replace the ohmic heating and the resulting degradation of the plasma confinement makes low temperature ignition difficult. The divertor plates must then handle large thermal heat fluxes. There is no demonstrated advantage to using divertors in high density plasmas, while the cumulative disadvantages make ignition difficult to attain. Their use would remove much of the rationale for using a compact, high field machine.

1.3.6 Time-dependent Ignition

The transient nature of ignition has important consequences. The initial current ramp, when I_p, n_e, B_T, and the plasma cross section are increased simultaneously, to their maximum values, has important effects on the plasma energy balance and stability at ignition.[57] These effects arise from the relatively slow inward diffusion of the plasma current, which is added at the outer surface of the plasma by the current ramp, compared to the growth of the central temperature due to plasma heating. The current ramp generates an inhomogeneous toroidal electric field in the plasma that is peaked near the plasma edge and allows large values of ohmic heating at high central temperature. The magnetic safety factor q can be easily maintained above unity or held to a very small $q < 1$ region during the current ramp. A more careful study,[57] shows that the magnetic safety factor can also be kept small after the ramp, at least until the central temperature reaches high values and fusion α-particles begin to appear, both of which are stabilizing effects for m = 1 modes. Furthermore, small amounts of injected heating (e.g., $P_{INJ} < P_{OH}/2$) during the current ramp can maintain a very small size (or nonexistence) for the $q < 1$ region until well past ignition, if central temperatures approach 10 keV by the end of the current ramp, through the freezing-in of the central current density at low resistivity. Injected heating also reduces the magnetic flux consumption required to reach ignition, particularly if ignition occurs during the current ramp. These characteristics are illustrated in table 1 (reference case for the maximum Ignitor design parameters, peak B_T= 13.5 T, I_p = 12 MA, R = 1.3 m, a = 0.48 m,

[57] B. Coppi, M. Nassi, and L.E. Sugiyama, *Physica Scripta* 45: 112 (1992);L. Sugiyama, and M. Nassi, *Nucl. Fusion* 32: 387 (1992).

κ= 1.8, and n_{eo}= 1.1 x 10^{21} m^{-3}, at 50:50 D:T ratio and Z_{eff} = 1.2).

It is possible to simultaneously maintain monotonically increasing q profiles without large low shear regions and with edge values $3 < q_{\psi a} < 4$ during the current ramp, to beyond ignition. These conditions should prevent instabilities associated with internal plasma modes (e.g., "locked" or quasistationary modes) that can be triggered during the current ramp and often lead to serious disruptions, in which the confinement of the plasma can be lost. Since hollow q profiles are usually associated with the excitation of internal macroscopic modes and enhanced, "anomalous" current penetration, while ignition is aided by a slow current penetration that keeps $q_o > 1$ for as long as possible, these precautions are not superfluous.

A major question for all ignition experiments is the degree of degradation expected in the plasma energy confinement near ignition, since D-T ignition is easily achieved if the confinement remains at the optimal ohmic heating level. One strategy for a high field experiment is to maintain a high level of ohmic heating up to ignition, $P_\alpha \leq 2P_{OH}$, to reduce the degree of degradation. Since α-particle heating possesses two important characteristics of ohmic heating that are not shared by any presently available form of injected heating—axisymmetric deposition and generation in the center of the plasma column—we expect that the degradation should not be as severe.

The requirement that the edge q is between 3 and 4 (high plasma current) means that special care must be devoted to maintaining q > 1 up to ignition. If only ohmic heating is contemplated, the steadily increasing size of the q < 1 region after the end of the current ramp imposes a more severe limit on the time in which the plasma can ignite and on the required energy confinement level than the energy balance alone. This assumes that sawtooth oscillations large enough to destroy the central peaking of the temperature cannot be avoided. Then ignition in the Ignitor reference case, at $T_o \approx 11$ keV, requires $\tau_E \approx 0.66$ seconds and must occur within approximately 1.5 seconds of the end of the current ramp (table 1). Our theoretical analysis, on the

Table 1. Reference Discharge for the Ignitor Ult. Maximum parameters at the End of Ramp I_p = 12 MA, B_T = 13.5 T, R = 1.3 m, a = 0.48 m, b = 0.87 m, $\delta \approx 0.4$, n_{eo} = 1.1 x 10^{21} m^{-3}, $n_{eo}/\langle n_e \rangle$ % = 2.2, Z_{eff} = 1.2.

	End Ramp	Ignition	
t	3.0	4.3	time (sec)
$\ell_i/2$	0.32	0.38	internal inductance
β_p	0.08	0.13	poloidal beta
β	0.8	1.26	toroidal beta (%)
$q_\psi\alpha$	3.3	3.6	edge magnetic safety factor
W	7.5	11.7	plasma kinetic energy (MJ)
T_{eo}	4.0	11.0	peak electron temperature (keV)
τ_E	710	660	energy confinement time (msec)
P_{OH}	13.0	9.5	ohmic heating (MW)
P_α	2.0	17.8	α-particle heating (MW)
$n_{\alpha o}$	1.5	12.0	peak α-particle density ($10^{17}m^{-3}$)
P_B	3.2	4.1	bremsstrahlung radiation (MW)
P_{IC}	0.4	0.5	cyclotron and impurity radiation (MW)
$V_{q=1}$	1.4	5.8	volume where q ≤ 1 (% of total)
$\Delta\Phi$	29.2	31.4	magnetic flux variation (V sec)
I_{BS}	0.6	1.0	bootstrap current (MA)

other hand, indicates that Ignitor remains, in all regimes, within the stability limits of the ideal MHD and resistive m = 1, n = 1 modes. In addition, moderate amounts of auxiliary heating, P_{ICRH} ~ 10-15 MW, started during the current ramp, allow ignition down to the limits predicted by $n_o\tau_E$, i.e., $\tau_E \leq 0.4$ sec, while maintaining very small q = 1 regions well beyond ignition. Similarly, in the ohmic case, if the requirement of small q < 1 region is dropped, either on the basis of the theoretical analysis or by externally stabilizing the sawtooth oscillations, ignition can also occur at this τ_E and at times of $t_i \approx$ 5-5.5 seconds.

The importance of ohmic heating during the ignition sequence at high field and density means that a model for the electron thermal transport should, similar to the one used here, simulate ohmic regimes and reproduce typical toroidal loop voltages in steady state ohmic experiments that are observed to be an almost "universal" constant. In addition, the total diffusion coefficient should increase with injected heating and reproduce the degraded confinement observed in present experiments that are dominated by injected heating.

A second major question for ignition is the effect of variation in the plasma density and its profile, since pellets injected to raise the density are unlikely to fully penetrate a high density plasma. For a given level of thermal transport, there is an optimum density for fastest ignition. A higher density is more favorable under degraded conditions. Higher density, however, accelerates the toroidal current penetration at a given time by lowering the T_e, producing larger q < 1 regions earlier than at lower density. This effect also operates in the outer part of the plasma radius when density profiles are broadened. Thus, for $n_{eo} = 1.1 \times 10^{21} m^{-3}$, profile peaking factors $n_{eo}/\langle n_e \rangle \geq 1.9$ where $\langle n_e \rangle$ is the volume average give relatively similiar results for ignition. Broader profiles rapidly lead to degraded ignition, e.g., $n_{eo}/\langle n_e \rangle = 1.5$ requires longer t_i and higher τ_E and yields a significantly larger q = 1 radius. Lower central density, e.g., $n_{eo} = 6.5 \times 10^{20} m^{-3}$ at the end of the current ramp increasing to 8-9 x 10^{20} by ignition, allows broader profiles, $n_{eo}/\langle n_e \rangle = 1.5$. For related reasons, increasing the plasma density after the current ramp is more advantageous than increasing the density during the ramp. At high density, a region of low magnetic shear develops in the mid-region of the minor radius. This region becomes seriously unstable when its value of q approaches unity, since ideal MHD instabilities with m = 1 can occur. This is one of the major limits on the broad density profile cases.

1.4 Versator II Tokamak Research Program

Sponsor

U.S Department of Energy
Contract DE-FG02-91-ER-54109

Project Staff

Professor Miklos Porkolab, Edward W. Fitzgerald, Jared P. Squire, Jesus Noel Villaseñor

Versator II is a small tokamak facility (major radius R = 40 cm, minor radius a = 13 cm) with modest plasma parameters (magnetic field B_0 ~ 1.3 Tesla, density $n_e \sim 3 \times 10^{13}$ cm^{-3}, and plasma current I_p ~ 10-80 kA) which is used for fundamental studies of the interaction of electromagnetic waves with a fully ionized, nearly collisionless plasma. For this purpose, we use several high power (P_{rf} ~ 100 kW) microwave sources to launch waves at frequencies near the electron-gyro frequency (f_{ce} ~ 28-35 GHz) and the lower hybrid (ion-plasma) frequency (f_o= 800 MHz or 2.45 GHz). In the sections below, we describe two different experimental projects which were carried out during the past year.

1.4.1 High Beta-Poloidal Experiments with Advanced X-Ray Diagnostics

High poloidal beta ($\varepsilon\beta \sim 1$) plasma equilibria have been produced by both toroidally asymmetric (current drive, LHCD) and symmetric (heating, LHH) lower hybrid RF injection in the Versator II tokamak. (Here β_p is the ratio of the plasma pressure to the poloidal magnetic field pressure, and $\varepsilon = a/R_0$ is the inverse aspect ratio). In both cases, the plasma current was fully sustained by the RF, with the loop voltage negligibly small (V_{loop}< 0.03V). The RF-created energy electron distribution function, which provides a large fraction of the plasma current and pressure in these plasmas, is studied by means of x-ray spectroscopy of the electron-ion bremsstrahlung plasma emission. Profile measurements of the emission perpendicular to the toroidal magnetic field and emission measurements at a full range of angles to the toroidal magnetic field have been carried out.

For low plasma current equilibria, β_p is enhanced, and an outward shift in major radius of the x-ray emission profile peak was observed, corresponding to a Shafranov shift ($\Delta_0/a \sim 0.33$) of the magnetic axis. The LHCD equilibrium current profile was determined from the x-ray emission profile. The safety factor on axis is calculated as $q_0 = 3 \pm 1$ and is nearly independent of the total current. The normal-

ized internal inductance increases slightly with lower plasma current, $l_i/2 = 0.8 \rightarrow 1.2$. From $\beta_p + l_i/2 \approx 4$, the poloidal beta is calculated, $\varepsilon\beta_p \cong 0.9$. The LHCD x-ray data indicate a highly anisotropic energetic electron distribution function with a density approximately 1 percent of the bulk electron density at the center. The stored energy of this distribution is much larger than the bulk energy and the global energy confinement time scales in agreement with the Kaye-Goldston L-mode scaling ($\tau_E \propto I_p^{1.2}$).

At high values of $\beta_p \sim 3$, LHH generates nearly the same plasma current as LHCD. The LHH equilibria has a reduction of up to a factor of four in the high energy (> 30 keV) x-ray emission flux, as compared to LHCD. Modeling of the electron distribution function in the LHH case indicates that only one third of the current is carried by the high energy electrons. At lower values of $\beta_p \sim 1.5$, LHH requires the assistance of a small applied loop voltage ($V_{loop} \sim 0.2V$) to maintain the plasma current. The high energy electrons carry a majority of the plasma current. Soft x-ray data indicates the presence of an enhanced intermediate energy electron population with a temperature of $T_{int} = 15$ keV. Calculations show that for the high $\beta_p \sim 3$ equilibria, the intermediate energy electrons could carry a majority of the current (~ 70%) in the form of bootstrap current.

Thesis

Squire, J.P. *An Experimental Study of Lower Hybrid Wave-driven High-Poloidal Beta Plasmas in the Versator II Tokamak.* Ph.D. diss., Dept. of Physics, MIT, 1993.

1.4.2 Fast Wave Current Drive Experiments

Previously we had discussed a combined fast wave-slow lower hybrid wave current drive experiment where two traveling waves are launched. Slow lower hybrid waves launched at 2.45 GHz by a conventional grill form a suprathermal electron tail, which is then expected to absorb an 800 MHz fast wave spectrum launched by a specially built dielectric-loaded waveguide array. This is expected to enhance the current driven by the 2.45 GHz slow wave, and raise the current drive efficiency at high densities where slow wave current drive efficiencies are degraded.

We have built and successfully tested the 800 MHz antenna, and showed that its coupling to the plasma corresponds well with theory. However, high power experiments ($P_{rf} < 25$ kW) using the fast wave antenna in conjunction with the 2.45 GHz launcher have failed to produce any form of current drive or central heating, as shown by measurements using tangential and perpendicular hard x-ray detectors. Further, only edge parameters appear to be affected with the application of RF power. Our code calculations indicate that according to linear wave theory, a significant fraction of the power should have penetrated the plasma interior and also should have been absorbed by fast electrons. We conclude that the fast waves must be absorbed on the plasma surface, possibly by non-linear effects such as parametric decay or scattering by low frequency edge density fluctuations.

Miniature retarding potential energy analyzer probes have been installed at different edge locations on Versator II. A thin region where electrons are heated from 5-10 eV to as high as 100 eV was detected. This region has a radial extent of approximately 1 cm, and a height of 2 cm, which corresponds to the antenna height. The region of hot electrons is located just behind the limiter edge and along the midplane of the tokamak (coplanar with the antenna array). This phenomena appears to be well localized in that region; no heating was seen in top or bottom probes. The heating also begins when the applied RF power exceeds 200 W.

We have also installed several electrostatic probes to measure the parametric decay spectra at different toroidal and poloidal locations. Parametric decay activity was clearly seen when the fast wave power is applied. We note asymmetric broadening of the pump frequency with more activity occuring on the lower frequency side of the pump. This phenomena has a measured threshold of $P_{rf} = 200$ W, which corresponds with the threshold of the edge electron heating.